

MCMC using *bouncy* Hamiltonian dynamics: A unifying framework for Hamiltonian Monte Carlo and piecewise deterministic Markov process samplers

Andrew Chin

Department of Biostatistics, Bloomberg School of Public Health,
Johns Hopkins University

and

Akihiko Nishimura

Department of Biostatistics, Bloomberg School of Public Health,
Johns Hopkins University

May 15, 2024

Abstract

Piecewise-deterministic Markov process (PDMP) samplers constitute a state of the art Markov chain Monte Carlo (MCMC) paradigm in Bayesian computation, with examples including the zig-zag and bouncy particle sampler (BPS). Recent work on the zig-zag has indicated its connection to Hamiltonian Monte Carlo, a version of the Metropolis algorithm that exploits Hamiltonian dynamics. Here we establish that, in fact, the connection between the paradigms extends far beyond the specific instance. The key lies in (1) the fact that any time-reversible deterministic dynamics provides a valid Metropolis proposal and (2) how PDMPs' characteristic velocity changes constitute an alternative to the usual acceptance-rejection. We turn this observation into a rigorous framework for constructing rejection-free Metropolis proposals based on *bouncy Hamiltonian dynamics* which simultaneously possess Hamiltonian-like properties and generate discontinuous trajectories similar in appearance to PDMPs. When combined with periodic refreshment of the inertia, the dynamics converge strongly to PDMP equivalents in the limit of increasingly frequent refreshment. We demonstrate the practical implications of this new paradigm, with a sampler based on a bouncy Hamiltonian dynamics closely related to the BPS. The resulting sampler exhibits competitive performance on challenging real-data posteriors involving tens of thousands of parameters.

Keywords: Bayesian statistics, generalized hybrid Monte Carlo, parameter constraints, event-driven Monte Carlo

1 Introduction

Markov Chain Monte Carlo plays a key role in Bayesian inference. The Metropolis-Hastings algorithm (Metropolis et al., 1953) provides a general recipe for constructing Markov chains with desired target distributions and has seen widespread use for Bayesian computation. However, traditional variants of Metropolis-Hastings can struggle in high-dimensional problems due to random walk behavior. This has led to increasing popularity of the modern variant known as Hamiltonian Monte Carlo (HMC) (Duane et al., 1987; Neal et al., 2011), especially with its adoption by probabilistic programming languages for applied Bayesian modeling (Carpenter et al., 2017; Salvatier et al., 2016). Hamiltonian Monte Carlo improves mixing by guiding exploration of the parameter space through Hamiltonian dynamics. These dynamics utilize the gradient of the target distribution to inform the evolution of an auxiliary momentum variable and thereby the sampler.

Recently, another sampling paradigm has emerged and garnered significant interest in the Bayesian computation community (Dunson and Johndrow, 2020). Built on the theory of piecewise-deterministic Markov processes (PDMP) (Davis, 1984; Fearnhead et al., 2018), the new paradigm includes the bouncy particle sampler (BPS) (Peters et al., 2012; Bouchard-Côté et al., 2018) and zig-zag sampler (Bierkens et al., 2019) as prominent examples. These samplers have origins in the non-reversible samplers of Diaconis et al. (2000), who, inspired by the role of momentum in HMC, introduced auxiliary variables that encode senses of direction to discrete-state Markov chains. These auxiliary variables correspond to velocity variables in PDMPs, which help suppress random walk behavior by promoting persistent motion in one direction at a time. Instantaneous changes in the velocities occur according to a Poisson process and ensure the correct stationary distribution.

Despite intense research efforts on both algorithms, there has been limited interaction

between the two fields. Previous connections include work of Nishimura et al. (2024), who establish a relationship between the zig-zag sampler and a novel variant of Hamiltonian Monte Carlo using Laplace distributed momentum. A relationship between HMC and the BPS appears as a high dimensional limit in Deligiannidis et al. (2021), who find that the first coordinate of the BPS process converges to Randomized HMC (Bou-Rabee and Sanz-Serna, 2017). However, this result only concerns a univariate marginal converging as the target dimension tends to infinity. Another critical distinction from our work is that Randomized HMC is actually an instance of a PDMP and is intrinsically stochastic. The algorithm gets its name because the differential equation underlying the PDMP admits an interpretation as Hamilton’s equations, but it lacks an arguably quintessential feature of the original HMC paradigm and its extensions (Fang et al., 2014): the use of a deterministic dynamics as a proposal mechanism.

In this work, we establish a single paradigm unifying the two. The unification critically relies on our construction of deterministic dynamics that (1) generate trajectories paralleling those of many PDMP samplers in appearance but (2) possess Hamiltonian-like properties allowing their use as a proposal mechanism within the Metropolis algorithm. We draw inspiration from existing ideas and distill them into two key aspects to construct this novel class of dynamics. The first idea is the concept of surrogate transition methods (Liu, 2001), which consider the use of generic time-reversible dynamics for proposal generation. HMC is a special case in which the dynamics generates rejection-free proposals in the absence of numerical approximation error. The method is more generally valid under arbitrary Hamiltonian-like dynamics, albeit without any guarantee of high acceptance rates. The second idea is that, in MCMC algorithms guided by an auxiliary velocity variable (Gustafson, 1998), an acceptance-rejection step can be replaced by a “bounce” event with

instantaneous changes in velocity preserving the target distribution. A continuous time limit of this idea is used by Peters et al. (2012) for motivating the BPS, though the idea has its roots as far back as event driven Monte Carlo of Alder and Wainwright (1959).

Our bouncy Hamiltonian dynamics combine the above two ideas by starting with Hamiltonian dynamics corresponding to a surrogate potential energy, which may or may not correspond to the target, and correcting for the surrogate’s deviation from the target through a deterministic bounce rule. We construct this deterministic bounce mechanism through a novel parameter augmentation scheme, introducing an inertia variable that evolves so as to exactly counterbalance discrepancies between the surrogate dynamics’s stationary distribution and the target. Our framework takes any position-velocity dynamics which is time-reversible, volume preserving, and energy conserving, and by bouncing when the inertia runs out, creates a rejection-free proposal mechanism.

These bouncy Hamiltonian dynamics generate trajectories reminiscent of and, in fact, possessing a direct connection to, PDMPs. By considering a modification in which the inertia variable is periodically refreshed, we show that the bouncy Hamiltonian dynamics converge strongly to PDMP counterparts in the limit of increasingly frequent inertia refreshment. The limiting class of processes is, unfortunately for the nomenclature, referred to as Hamiltonian PD-MCMC by Vanetti et al. (2017), and encompasses the BPS as well as the Boomerang sampler of Bierkens et al. (2020)

After establishing the general theory, we turn to demonstrating its practical implications by studying a sampler based on a specific bouncy Hamiltonian dynamics. We refer to this sampler as the Hamiltonian bouncy particle sampler (HBPS), as its refreshment limit coincides with the BPS. We prove that, despite all its Hamiltonian-like properties, the dynamics does not admit an interpretation as a bona fide Hamiltonian dynamics in the

classical sense. Our bouncy Hamiltonian dynamics thus provides an entirely new proposal generation mechanism and expands the existing tool kit for Bayesian computation.

We demonstrate the HBPS’s competitive performance on two high-dimensional posteriors from modern real-data applications: a sparse logistic regression for an observational study comparing blood anti-coagulants (Tian et al., 2018) and a phylogenetic probit model applied to HIV data (Zhang et al., 2021). Posterior computations for these models rely on Gibbs samplers whose conditional updates include challenging 22,174 dimensional and 11,235 dimensional targets. When applied to these conditional updates, our sampler shows superior performance against alternatives and is far easier to tune than the BPS.

We close with two extensions of the bouncy Hamiltonian dynamics. We first introduce a numerical approximation method that enables use of our dynamics when exact solutions for the surrogate dynamics or bounce times are not available. We then discuss an analog of local PDMP methods (Bouchard-Côté et al., 2018; Vanetti et al., 2017) when the target density is a product of factors. This framework subsumes the Hamiltonian zig-zag (Nishimura et al., 2024), which arises as a local version of the HBPS.

2 Background

2.1 Hamiltonian Monte Carlo and use of time-reversible dynamics to generate Metropolis proposals

We start this section by reviewing the standard Hamiltonian Monte Carlo algorithm and proceed to describe how time-reversible, volume preserving dynamics can be used to construct Metropolis proposals more generally.

We denote a target distribution as $\pi(x)$, which may be unnormalized, for a parameter of

interest $x \in \mathbb{R}^d$. HMC is a version of the Metropolis algorithm which proposes new states through simulation of Hamiltonian dynamics. To do this, it augments the target with an auxiliary momentum variable $p \in \mathbb{R}^d$ and targets the joint distribution $\pi(x, p) = \pi(x)\pi(p)$.

Each iteration of HMC follows a two step process. First, the current momentum value is discarded and a new value p_0 is drawn from its marginal $\pi(p)$. Second, combining the new momentum with the current position to form an initial state (x_0, p_0) , Hamiltonian dynamics defined by the following differential equations are simulated for a set time T :

$$\frac{dx}{dt} = \frac{\partial}{\partial p}K(p), \quad \frac{dp}{dt} = -\frac{\partial}{\partial x}U(x), \quad (1)$$

with the kinetic energy $K(p) = -\log \pi(p)$ and potential energy $U(x)$ which, in the standard Hamiltonian Monte Carlo setting, is taken as $U(x) = -\log \pi(x)$. The state of the dynamics at the final time point, (x_T, p_T) , is then used as a proposal and accepted with the standard Metropolis probability $\min\{1, \pi(x_T, p_T)/\pi(x_0, p_0)\}$. Note that the proposal generation step is completely deterministic; randomness in HMC comes only from the momentum refreshment step.

Hamiltonian dynamics exhibits a number of key properties that makes it suitable for generating proposals. The dynamics is time-reversible and volume preserving, thereby constituting a Metropolis proposal mechanism. Additionally, the dynamics is energy conserving: the sum of the potential and kinetic energies is constant along its trajectories. Since $\pi(x, p) = \exp(-[U(x) + K(p)])$, the energy conservation implies $\pi(x_T, p_T) = \pi(x_0, p_0)$ and makes HMC proposals rejection-free when the dynamics is simulated exactly. In particular, this property serves as an important inspiration in our construction in Section 3 of bouncy Hamiltonian dynamics; the surrogate dynamics on its own does not preserve the total energy, but the energy conservation is imposed via the additional inertia variable.

While HMC and most of its variants take the potential energy U in Equation (1) to

coincide with $-\log \pi(x)$, Hamiltonian dynamics remain a valid proposal under *any* choice of U . When considering this more general use case, we refer to Hamiltonian dynamics used to generate proposals as *surrogate* dynamics. And, to clearly distinguish the potential energy underlying surrogate dynamics and the negative log density of the target, we denote the former as U_{sur} , the latter U_{tar} , and their difference $U_{\text{dif}} = U_{\text{tar}} - U_{\text{sur}}$. The surrogate dynamics preserves the quantity $U_{\text{sur}}(x) + K(p)$ along the trajectory and hence the acceptance probability can be expressed as

$$\min\{1, \exp(-[U_{\text{dif}}(x_T) - U_{\text{dif}}(x_0)])\}. \quad (2)$$

When taking a flat potential $U_{\text{sur}} = 0$, for example, the surrogate dynamics yield linear trajectories that underlie the BPS; an implication of this fact is explored in Section 4.1.

The potential use of arbitrary Hamiltonian dynamics as a proposal mechanism has not received much attention in the HMC literature, where most research has focused on how to pick the momentum distribution $\pi(p)$ (Girolami and Calderhead, 2011; Livingstone et al., 2019b) and how to numerically approximate the dynamics efficiently (Blanes et al., 2014; Bou-Rabee and Sanz-Serna, 2018). As we dissect PDMPs in the next section, the surrogate transition perspective helps us view its bounce mechanism as an alternative to an acceptance-rejection procedure.

2.2 Piecewise-deterministic Markov processes as continuous limit of Metropolis moves and delayed-rejection bounces

In contrast to deterministic Hamiltonian dynamics, PDMPs are continuous time stochastic processes which achieve guided exploration of the original parameter space through an auxiliary velocity variable v . PDMPs target the joint distribution $\pi(x)\pi(v)$ by combining

deterministic dynamics with an inhomogeneous Poisson process that causes random changes in velocity.

A general class of PDMPs, which subsumes a number of prominent examples, is presented by Vanetti et al. (2017) and is given the name, unfortunately for the nomenclature, Hamiltonian PD-MCMC. These PDMPs are so called because they use Hamiltonian dynamics as their deterministic components. Different choices of potential energy $U_{\text{sur}}(x)$ given rise to different variants but the kinetic energy is fixed as $K(v) = \|v\|^2/2$, corresponding to the standard Gaussian distribution for v . Hamiltonian PD-MCMC hence uses the deterministic dynamics

$$\frac{dx}{dt} = v_t, \quad \frac{dv}{dt} = -\nabla U(x_t). \quad (3)$$

We note that referring to the auxiliary variable as “velocity” here is appropriate since the notions of momentum and velocity in Hamiltonian dynamics coincide when assuming the standard Gaussian density for the auxiliary variable. In other words, if we define the auxiliary variable as “momentum” p and the quantity $\frac{\partial}{\partial p} K(p)$ providing the time derivative dx/dt in Equation (1) as “velocity” v , then we indeed have $p = v$ when $K(p) = -\log \pi(p) = \|p\|^2/2$.

The deterministic component of Hamiltonian PD-MCMC plays a role analogous to the surrogate dynamics providing a proposal mechanism as introduced in Section 2.1. Instead of the acceptance-rejection used by the surrogate transition method, however, Hamiltonian PD-MCMC introduces velocity switch events along the trajectory to preserve the target. These events occur according to the arrival times of an inhomogeneous Poisson process. To highlight resemblance to the surrogate transition method, we now reintroduce notation from Section 2.1. We refer to the potential energy U underlying the deterministic component as U_{sur} and set $U_{\text{tar}} = -\log \pi(x)$, so $U_{\text{dif}} = U_{\text{tar}} - U_{\text{sur}} = -\log \pi(x) - U$. With this notation,

the Poisson rate for velocity switches in Hamiltonian PD-MCMC is given by

$$\lambda(t) = \lambda(x_t, v_t) = [v_t^\top \nabla U_{\text{dif}}(x_t)]^+ = \left[\frac{d}{ds} U_{\text{dif}}(x_t) \Big|_{s=t} \right]^+ \quad (4)$$

and can be seen clearly as a function of the discrepancy between the surrogate and target.

By a property of Poisson processes, the velocity switch event time can be simulated by drawing an exponential random variable ε with unit rate and then solving for

$$t_B^* = \inf_{t>0} \left\{ \varepsilon = \int_0^t [v_t^\top \nabla U_{\text{dif}}(x_t)]^+ ds \right\}. \quad (5)$$

At time t_B^* , Hamiltonian PD-MCMC undergoes an instantaneous change in the velocity $v \leftarrow R_x(v)$ in the form of an elastic bounce off the hyperplane orthogonal to ∇U_{dif} , where the reflection function $R_x(v)$ is defined by

$$R_x(v) = v - 2 \frac{v^\top \nabla U_{\text{dif}}(x)}{\|\nabla U_{\text{dif}}(x)\|^2} \nabla U_{\text{dif}}(x). \quad (6)$$

Hamiltonian PD-MCMC as prescribed above samples from the given target as can be verified, *after the fact*, straightforwardly with the theory of Markov jump processes and Kolmogorov’s equations (Fearnhead et al., 2018). However, it is apposite to ask: where does the algorithm come from in the first place? In tracing the historical development of PDMP, we find the algorithm to emerge from two key ideas. The first is to guide a Markov chain’s movement via an auxiliary variable to promote persistent motion (Diaconis et al., 2000), and this idea’s connection to PDMPs is most clearly seen in the guided random walk of Gustafson (1998). The second is the idea of “event-driven” moves as alternatives to acceptance-rejection (Alder and Wainwright, 1959; Peters et al., 2012) which, in statistical language, can be interpreted as a delayed-rejection scheme (Mira et al., 2001; Sherlock and Thiery, 2022).

The guided random walk uses an auxiliary direction variable v and makes moves in the position-velocity space. We present a multivariate version of the algorithm which is an

extension of the original work by Gustafson (1998) implicitly used by Sherlock and Thiery (2022). The algorithm draws the auxiliary variable $v \in \mathbb{R}^d$ from a standard multivariate Gaussian and makes a move the form:

$$(x_{\Delta t}^{n+1}, v_{\Delta t}^{n+1}) = \begin{cases} (x_{\Delta t}^n + \Delta t v_{\Delta t}^n, v_{\Delta t}^n) & \text{with probability } \min \left\{ 1, \frac{\pi(x_{\Delta t}^n + \Delta t v_{\Delta t}^n)}{\pi(x_{\Delta t}^n)} \right\} \\ (x_{\Delta t}^n, -v_{\Delta t}^n) & \text{otherwise.} \end{cases} \quad (7)$$

Crucially, when proposals are accepted, v is maintained so the subsequent proposal is again in the same direction; when proposals are rejected, v is negated so the next proposal is in the reverse direction.

The proposal $x_n + \Delta t v_n$ can be viewed as simulating Gaussian momentum based Hamiltonian dynamics for time Δt on a flat potential with initial position and velocity (x_n, v_n) . This perspective allows us to generalize the guided random walk to use Hamiltonian dynamics with arbitrary potential U_{sur} . Let $\Phi(t, x, v) : \mathbb{R}^{2d+1} \rightarrow \mathbb{R}^d$ denote the *solution operator* of this dynamics, which takes an initial state (x, v) , and returns the state (x_t, v_t) obtained as a result of simulating the dynamics for time t . Our generalized guided random walk proposes a Hamiltonian move $(x'_{\Delta t}, v'_{\Delta t}) = \Phi(\Delta t, x, v)$ and accepts it with probability

$$\min\{1, \exp(-[U_{\text{dif}}(x'_{\Delta t}) - U_{\text{dif}}(x)])\}$$

or negates the velocity otherwise. This results in a Markov chain which starts backtracking the trajectory of Hamiltonian dynamics upon rejection.

In the limit $\Delta t \rightarrow 0$, this process converges to a continuous time Markov chain where the velocity flips at the first arrival time of a Poisson process with rate given in Equation (4).

This can be seen by applying second order Taylor expansions to the acceptance probability:

$$\begin{aligned}
\min\{1, \exp(-[U_{\text{dif}}(x'_{\Delta t}) - U_{\text{dif}}(x)])\} &= \exp(-[U_{\text{dif}}(x'_{\Delta t}) - U_{\text{dif}}(x)]^+) \\
&= \exp(-[\Delta t(v^\top \nabla U_{\text{dif}}(x)) + O(\Delta t^2)]^+) \\
&= 1 - \Delta t[v^\top \nabla U_{\text{dif}}(x)]^+ + O(\Delta t^2).
\end{aligned}$$

The rejection probability for each move is thus approximately $\Delta t[v^\top \nabla U_{\text{dif}}(x)]^+$, and there are $\lfloor T/\Delta t \rfloor$ attempted moves when simulating the dynamics for duration T .

To avoid the backtracking behavior, which restricts exploration to one dimension, we introduce the second key idea of event-driven bounces as an alternative to simply negating the velocity. More precisely, we incorporate the reflective bounce of Equation (6) into the guided Markov chain using a delayed rejection scheme. Upon rejection, we can generate a new proposal $(x''_{\Delta t}, v''_{\Delta t}) = \Phi(\Delta t, x'_{\Delta t}, R_{x'_{\Delta t}}(v'_{\Delta t}))$ to be accepted with probability (Mira et al., 2001; Sherlock and Thiery, 2022)

$$\frac{1 - e^{-[U_{\text{dif}}(x''_{\Delta t}) - U_{\text{dif}}(x'_{\Delta t})]^+} e^{-U_{\text{tar}}(x''_{\Delta t})}}{1 - e^{-[U_{\text{dif}}(x'_{\Delta t}) - U_{\text{dif}}(x)]^+} e^{-U_{\text{tar}}(x)}}.$$

In the guided walk's continuous limit $\Delta t \rightarrow 0$, the above acceptance probability converges to $R_x(-v)^\top \nabla U_{\text{dif}}(x) / v^\top \nabla U_{\text{dif}}(x) = 1$ and results in a bounce event that occurs according to the Poisson rate (4).

The above construction shows Hamiltonian PD-MCMC as a limit of a discrete-time Markov chain guided by surrogate Hamiltonian dynamics combined with delayed-rejection bounces. The derivation of the BPS as a continuous limit in Peters et al. (2012) and Sherlock and Thiery (2022) can be viewed as a special case in which the surrogate Hamiltonian dynamics corresponds to a trivial one with $U_{\text{sur}} = 0$.

3 Bouncy Hamiltonian Dynamics

3.1 Constructing rejection-free dynamics by synthesizing surrogate dynamics with event-driven bounces

The surrogate method discussed in Section 2.1 generates proposals using surrogate dynamics with potential energy U_{sur} and corrects for the discrepancy between U_{sur} and U_{tar} via acceptance-rejection. The acceptance probability in Equation (2) degrades as the discrepancy grows, leading to a large proportion of rejections and inefficient exploration. Here we show that acceptance-rejection can be replaced by deterministic bounces in the trajectory. This resulting dynamics piecewise follow the surrogate dynamics in between deterministic bounces and generate rejection-free proposals.

Our construction of bouncy Hamiltonian dynamics starts with surrogate dynamics, whose trajectory (x_t, v_t) is given by the solution to Equation (1) with surrogate potential $U_{\text{sur}}(x)$ and kinetic energy $K(v) = \|v\|^2/2$. In introducing deterministic bounces, we take inspiration from Nishimura et al. (2024), who find that Hamiltonian dynamics with Laplace distributed momentum yields trajectories akin to the zig-zag process. Crucially, they find this Hamiltonian dynamics to undergo an instantaneous velocity switch at the moment when momentum runs out along a coordinate. Emulating this behavior, we introduce an inertia variable $l \geq 0$ that is exponentially distributed with unit rate and define the bounce time as the moment when the inertia runs out. The dynamics operate in \mathbb{R}^{2d+1} to target the joint distribution $\pi(x, v, l) = \pi(x)\pi(v)\pi(l)$, whose negative log density is $U_{\text{tar}}(x) + K(v) + l$. This inertia will play the role of a pseudo-momentum, and, additionally, evolve so as to conserve the joint density $\pi(x, v, l)$.

From an initial state (x_0, v_0, l_0) , we let the position-velocity component (x_t, v_t) evolve

according to the surrogate dynamics. In the meantime, we define the evolution of the inertia component as

$$l_t = l_0 - \int_0^t v_s^\top \nabla U_{\text{dif}}(x_s) \, ds = l_0 + U_{\text{dif}}(x_0) - U_{\text{dif}}(x_t). \quad (8)$$

Where we denote $U_{\text{dif}} = U_{\text{tar}} - U_{\text{sur}}$ as before. With this specification, the inertia runs out at time

$$t^* = \inf_{t>0} \left\{ l_0 = \int_0^t v_s^\top \nabla U_{\text{dif}}(x_s) \, ds = U_{\text{dif}}(x_t) - U_{\text{dif}}(x_0) \right\}. \quad (9)$$

At time t^* , a reflection occurs against ∇U_{dif} in the manner of Equation (6), emulating the bounce of the PDMP. The process for simulating the dynamics for duration T is summarized in Algorithm 1, where $\Phi(t, x, v)$ denotes the solution operator of the surrogate dynamics. The bouncy Hamiltonian dynamics as constructed maintains the surrogate dynamics' ability to generate valid proposals and, further, makes proposals rejection-free by exactly compensating for the discrepancy between the surrogate and target potential:

Theorem 1 *Assume that U_{sur} is twice continuously differentiable and the set $\{x : \nabla U_{\text{sur}}(x) = 0\}$ consists of smooth manifolds of dimension at most $d - 1$. Then, for any initial condition away from a set of measure 0, the bouncy Hamiltonian dynamics on \mathbb{R}^{2d+1} are time-reversible, volume preserving, and preserve the augmented energy $U_{\text{tar}}(x) + K(v) + l = -\log \pi(x, v, l)$.*

The proof is in Supplement Section 1. The properties established by Theorem 1 imply our bouncy dynamics constitute a valid Metropolis proposal mechanism. We also note that the bouncy Hamiltonian dynamics straightforwardly extend to accommodate parameter constraints by elastically reflecting off any boundaries encountered in the same manner as in standard Hamiltonian dynamics and PDMPs (Neal et al., 2011; Bierkens et al., 2018).

We close this section by discussing notable special cases of bouncy Hamiltonian dynamics. When setting $U_{\text{sur}} = U_{\text{tar}}$, no bounce ever occurs because $U_{\text{dif}} = 0$ and we recover classical, smooth Hamiltonian dynamics. The choice $U_{\text{sur}} = \|x\|^2/2$ yields dynamics whose trajectories parallel those of the Boomerang sampler (Bierkens et al., 2020); this bouncy dynamics can be used to construct an analogue of the Boomerang sampler, though we do not pursue this possibility here. Instead, for the rest of this article, we focus on the case $U_{\text{sur}} = 0$. This yields a bouncy Hamiltonian analogue of the BPS’s piecewise linear dynamics with constant velocity, which we call HBPS dynamics. We study this dynamics and resulting sampler further in Section 4.

Algorithm 1 BouncyHamiltonian

Dynamics(T, x, v, l) $\tau \leftarrow 0$ \triangleright current time traveled**while** $\tau < T$ **do**

$$t^* = \inf_{t>0} \{l = \int_0^t v_{\tau+s}^\top \nabla U(x_{\tau+s}) ds\}$$

if $\tau + t^* > T$ **then**

$$x_T, v_T \leftarrow \Phi(T - \tau, x, v)$$

$$l_T \leftarrow l_\tau - \int_0^{T-\tau} v_{\tau+s}^\top \nabla U(x_{\tau+s}) ds$$

return x_T, v_T, l_T **else**

$$x_{\tau+t^*}, v_{\tau+t^*} \leftarrow \Phi(t^*, x_\tau, v_\tau)$$

$$v_{\tau+t^*} \leftarrow R_{x_{\tau+t^*}}(v_{\tau+t^*})$$

$$l_{\tau+t^*} \leftarrow 0$$

$$\tau \leftarrow \tau + t^*$$

end if**end while**

Algorithm 2 Bouncy Hamiltonian sam-

pler for n iterations.**Require:** x, T, n **for** $i = 1, \dots, n$ **do**Draw $v \sim N(0, I^d)$ Draw $l \sim \text{Exp}(1)$ $x, v, l \leftarrow$ BouncyHamiltonianDynamics(T, x, v, l) \triangleright Algorithm 1Store x as sample**end for**

3.2 Piecewise-deterministic Markov processes as a limit

The trajectories of the bouncy Hamiltonian dynamics and its PDMP counterpart have much in common: both follow the same deterministic dynamics between events and undergo bounces in an identical manner. On the other hand, the two dynamics differ in how event times are determined: one follows a deterministic process dictated by the inertia variable while the other a Poisson schedule dictated by exponential random variables.

We now present a theoretical result that quantifies a relationship between the two dynamics. To this end, we consider modifying bouncy Hamiltonian dynamics by adding

resampling of inertia from its marginal at regular intervals of size Δt . This refreshment of inertia introduces randomness in otherwise deterministic bounce times. As we increase the frequency of this refreshment by letting $\Delta t \rightarrow 0$, the next bounce time becomes effectively independent of the past evolution, making the dynamics Markovian. In fact, in this limit, the dynamics converges in its position and velocity components to its PDMP counterpart. To state the result more formally, let $D[0, \infty)$ denote the space of right-continuous-with-left-limit functions from $[0, \infty) \rightarrow \mathbb{R}^d \times \mathbb{R}^d$ with the Skorokhod topology (Billingsley, 1999; Ethier and Kurtz, 2009). We also make a common assumption in the HMC literature to control the dynamics's behavior in the tails (Livingstone et al., 2019a), which roughly says the density proportional to $\exp(-U_{\text{sur}})$ has tails no lighter than exponential. We then have the following result:

Theorem 2 (Weak Convergence) *Assume U_{sur} and U_{tar} are twice continuously differentiable and $\limsup_{\|x\| \rightarrow \infty} \frac{\|\nabla U_{\text{sur}}(x)\|}{\|x\|} < \infty$. Consider a sequence of bouncy Hamiltonian dynamics, indexed by $\Delta t > 0$, with a common initial position and velocity (x_0, v_0) but with the added inertia refreshment at every Δt interval. Let $(x_{\Delta t}^H, v_{\Delta t}^H)$ denote the position and velocity components of these dynamics. As $\Delta t \rightarrow 0$, the dynamics converge weakly in $D[0, \infty)$ to corresponding PDMP with the same initial condition and inter-bounce dynamics governed by the surrogate Hamiltonian dynamics.*

In fact, the above result is a consequence of a stronger convergence result below.

Theorem 3 (Strong Convergence) *Under the same assumptions as in Theorem 2, the position-velocity components $(x_{\Delta t}^H, v_{\Delta t}^H)$ of the bouncy Hamiltonian dynamics with inertia refreshment converge strongly to the same corresponding PDMP limit in $D[0, T]$ for any $T > 0$.*

More precisely, we can construct a sequence of PDMPs $(x_{\Delta t}^P, v_{\Delta t}^P)$ having the same distribution as the limiting PDMP, where each is coupled to the bouncy Hamiltonian dynamics such that

$$\lim_{\Delta t \rightarrow 0} \mathbb{P}[\rho_T\{(x_{\Delta t}^H, v_{\Delta t}^H), (x_{\Delta t}^P, v_{\Delta t}^P) > \epsilon\}] = 1,$$

where ρ_T denotes the Skhorokod metric on $[0, T]$.

Since the strong convergence holds for any $T > 0$, Theorem 3 implies the weak convergence result of Theorem 2 (Billingsley, 1999). The proof of Theorem 3 is in Supplement Section 2.

The theorem shows that bouncy Hamiltonian dynamics not only generalize classical Hamiltonian dynamics, but also recover PDMPs in the limit, thereby unifying the HMC and PDMP paradigms. One implication is that the theoretical performance of the two paradigms may be closely related. On the other hand, as we demonstrate in Section 5, their deterministic and stochastic nature result in significant differences in their practical performance.

4 The Hamiltonian bouncy particle sampler

4.1 Bouncy Hamiltonian dynamics underlying the sampler

The BPS is an instance of a Hamiltonian PD-MCMC algorithm as described in Section 2.2 with the surrogate dynamics corresponding to a constant potential. Since the dynamics is only affected up to additive constants, we assume without loss of generality that $U_{\text{sur}} = 0$ and $U_{\text{dif}} = U_{\text{tar}}$. The differential equation (3) governing the deterministic part in this case becomes

$$\frac{dx}{dt} = \frac{\partial}{\partial v} \frac{\|v\|^2}{2} = v, \quad \frac{dv}{dt} = -\frac{\partial}{\partial x} 0 = 0,$$

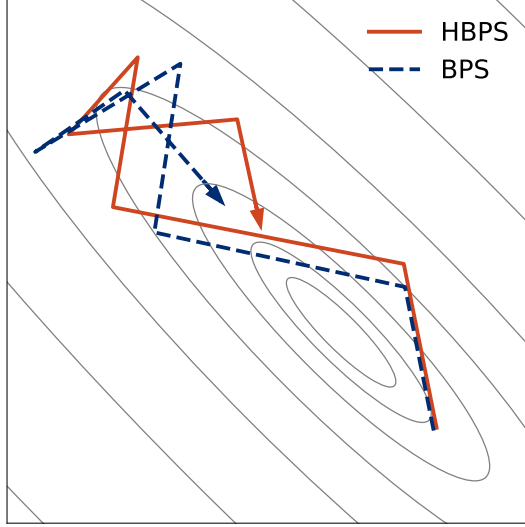


Figure 1: Trajectories of the HBPS dynamics (solid red) and the BPS's dynamics (dashed blue) from the same initial position and velocity on a correlated bivariate Gaussian target.

From a given initial position and velocity (x_0, v_0) , therefore, the dynamics evolves as

$$x_t = x_0 + tv_0, \quad v_t = v_0$$

until velocity switch events that occur according to the rate

$$\lambda(t) = [v_0^\top \nabla U_{\text{tar}}(x_0 + tv_0)]^+. \quad (10)$$

We now replace the Poisson bounce events of the BPS with our deterministic inertia-driven process. This yields bouncy Hamiltonian dynamics whose evolution, following Equation (8) and (9), takes the following form. Prior to a bounce event, the dynamics evolves as

$$\begin{aligned} x_t &= x_0 + tv_0, \quad v_t = v_0 \\ l_t &= l_0 - \int_0^t v_0^\top \nabla U_{\text{tar}}(x_0 + sv_0) ds = l_0 + U_{\text{tar}}(x_0) - U_{\text{tar}}(x_0 + tv_0). \end{aligned} \quad (11)$$

The bounce event occurs when the inertia runs out at time t^* , given by

$$t^* = \inf_{t>0} \left\{ l_0 = \int_0^t v_0^\top \nabla U_{\text{tar}}(x_0 + sv_0) ds = U_{\text{tar}}(x_0 + tv_0) - U_{\text{tar}}(x_0) \right\}. \quad (12)$$

At time t^* , the velocity is reflected in exactly the same manner as the BPS:

$$x^* = x_0 + t^* v_0, \quad v^* = R_{x^*}(v_0), \quad t^* = 0.$$

With this new state, the next event time is computed and the process is repeated. Figure 1 compares an example trajectory to the BPS’s.

Thanks to Theorem 1, the above dynamics can be used as a valid proposal to yield a version of the bouncy Hamiltonian sampler, which we term the *Hamiltonian bouncy particle sampler* (HBPS). We refer to the underlying dynamics given by Equations (11) and (12) as *HBPS dynamics*.

4.2 Is it Hamiltonian dynamics in disguise?

The prior work of Nishimura et al. (2024) suggests a potential connection between HMC and PDMPs by identifying a novel variant of Hamiltonian dynamics with highly unusual “bouncy” behavior. It is apposite to ask, therefore, whether our bouncy Hamiltonian dynamics can also be described within the existing framework if viewed from a right perspective. We show this *not* to be the case for the HBPS dynamics and hence for bouncy Hamiltonian dynamics in general. Our bouncy dynamics thus provides a fundamentally new tool for proposal generation in Bayesian computation.

When considering a univariate target density $\pi(x)$, Nishimura et al. (2024)’s Hamiltonian zig-zag coincides with HBPS dynamics in their position-velocity components. This is analogous to how the zig-zag sampler and BPS coincide in one dimension (Bierkens et al., 2019). In higher dimensions, however, no Hamiltonian dynamics is capable of emulating HBPS dynamics’ piecewise linear trajectory in the position space. In particular, we show that, in contrast to how the Laplace momentum yields Hamiltonian zigzag, no choice of momentum distribution yields HBPS dynamics:

Theorem 4 *Suppose a given target $\pi(x)$ in \mathbb{R}^d for $d \geq 3$ is strongly log-concave. Then no choice of smooth momentum distribution $\pi(p)$, even allowing for discontinuities in between piecewise smooth components, yields Hamiltonian dynamics that parallels HBPS’s piecewise linear dynamics in the position component.*

The precise meaning of “Hamiltonian dynamics” in the theorem statement warrants clarification. The classical Hamiltonian dynamics are guaranteed to generate smooth trajectories and cannot possibly emulate HBPS’s discontinuous change in velocity. The theorem thus considers a more general class of *discontinuous* Hamiltonian dynamics, in which discontinuous behavior becomes possible through discontinuity in the gradient of the kinetic energy (Nishimura et al., 2020). The theorem, with proof in Supplement Section 3, establishes that HBPS dynamics lies outside this even broader class of dynamics.

4.3 Efficient implementation on constrained log-concave targets

HBPS dynamics is of particular interest as it permits exact simulation on log-concave targets. Given a user-specified total travel time T , each iteration of the sampler involves refreshing the auxiliary velocity and inertia, and then simulating the dynamics for user-specified duration T from the current state x . The end positions of the trajectories are kept as samples. Algorithm 2 provides the recipe to run n iterations of the sampler.

Our dynamics’s deterministic and time-reversible nature also makes it possible to take advantage of the No-U-Turn algorithm of Hoffman et al. (2014) to minimize tuning. This algorithm only requires a base unit of step size as an input and multiplicatively adapts the total travel time for efficient exploration while preserving detailed balance. The base step size can be chosen either heuristically or adaptively (Nishimura et al., 2024). The combination of the HBPS dynamics with No-U-Turn results in a sampler with minimal

user input. This sampler in particular excels in Gibbs sampling schemes where the conditional posteriors change at each iteration and may require varying travel times for optimal exploration of the conditional.

Simulating the HBPS is more computationally efficient than simulating the BPS on log-concave targets. Solving for the BPS’s event time t_B^* in Equation (5), which contains a positive-part operator in the integrand, requires a minimization first to find the time t_{min}^* at which the directional derivative turns positive (Bouchard-Côté et al., 2018):

$$t_{min}^* = \inf_{t>0} \{v_0^\top \nabla U_{tar}(x_0 + tv_0) \geq 0\}.$$

Then, an additional root finding procedure is required to find t_B^* :

$$t_B^* = \inf_{t>t_{min}^*} \left\{ \varepsilon = \int_{t_{min}^*}^t v_0^\top \nabla U_{tar}(x_0 + sv_0) ds = U_{tar}(x_0 + tv_0) - U_{tar}(x_0 + t_{min}^* v_0) \right\}.$$

On the other hand, computing bounces times for the HBPS requires only a single root finding algorithm to solve Equation (12), bypassing the need for the minimization. This significantly reduces the number of numerical operations required relative to the BPS.

For our applications, we solve for the roots using the Newton–Raphson algorithm for both samplers. Minima for the BPS are found using the Broyden–Fletcher–Goldfarb–Shanno algorithm (Wright et al., 1999), which we find to be faster for our applications than Newton–Raphson.

Constraints on the position parameter of the target can be handled in the same way as the BPS by elastically bouncing off of the boundaries (Bouchard-Côté et al., 2018). The required computation of boundary event times is trivial as both samplers have constant velocities.

5 Applications

5.1 Setup

We compare the HBPS against other algorithms on two challenging real-data applications. In each example, the joint posterior distribution is difficult to sample from directly, but the conditional distributions are more tractable. We thus employ a Gibbs scheme where the computational bottleneck is a high dimensional log-concave distribution. We apply the HBPS and alternative algorithms to this conditional update and compare variations of the Gibbs samplers differing only in this aspect. Performance is measured using effective sample size (ESS) calculated by the method of Plummer et al. (2006) and normalized by computation time. We measure ESS across the parameters of interest and then use the minimum value achieved, representing how effectively the algorithm sampled the most difficult parameter. Final results are averaged over five runs with different seeds. We present ESS per time relative to the performance of the BPS to facilitate comparisons, with BPS taking the value of 1 and higher values indicating higher ESS per time.

The comparisons feature three algorithms with increasing numbers of tuning parameters: the HBPS with No-U-Turn algorithm, the HBPS with manually tuned travel time, and the BPS with manually tuned travel time and refresh rate. The refresh rate is necessitated by the known risk of BPS’s reducible behavior when using the event rate in Equation (10) on its own (Bouchard-Côté et al., 2018). The sampler is thus typically implemented with additional velocity refreshment by introducing a refresh rate λ_{ref} and setting $\lambda(t) = \lambda_{tar}(t) + \lambda_{ref}$. At the first arrival time t^* of this combined rate, the process refreshes the velocity with probability $\lambda_{ref}/\lambda(t^*)$ or bounces otherwise.

The base step size for the No-U-Turn algorithm is chosen as suggested in Nishimura et al.

(2024) by estimating the covariance matrix, computing the maximum eigenvalue λ_{max} , and then using $0.1\sqrt{\lambda_{max}}$. No further tuning for the No-U-Turn algorithm is done to treat it as an option with minimal need for user input. For tuning of the HBPS, we start with the average travel time T selected by the No-U-Turn algorithm as our starting point. Then we search a grid of travel times of $T \pm jT/4$, for $j = 0, 1, 2, 3$.

We run simulations on the Joint High Performance Computing Exchange cluster at Johns Hopkins, allocating a single AMD EPYC 7713 CPU core and 32 gigabytes of memory for each chain.

5.2 Bayesian sparse logistic regression: conditionally log-concave target

The first posterior distribution arises from an observational study comparing the risk of gastrointestinal bleeding from two alternative blood anticoagulants, dabigatran and warfarin. The study is based on the new-user cohort design and includes of 72,489 patients and 22,174 covariates extracted from the Merative MarketScan Medicare Supplemental and Coordination of Benefits Database. As part of the average treatment effect estimation, propensity scores (Rosenbaum and Rubin, 1983) are estimated with a Bayesian sparse logistic regression model, the required posterior computation for which we compare our samplers on.

The probability of taking dabigatran is modeled via logistic regression:

$$\text{logit}\{p_i(\beta)\} = \text{logit}\{\mathbb{P}(i\text{-th patient on dabigatran)}\} = x_i^\top \beta.$$

The regression coefficients β_j are given a bridge prior (Polson et al., 2013) to induce sparsity in the posterior estimates. Under the global-local representation, commonly used to facilitate the posterior computation, the prior is parametrized with global and local scale

τ and λ_j as:

$$\beta_j \mid \tau, \lambda_j \sim N(0, \tau^2 \lambda_j^2), \quad \tau \sim \pi_{\text{global}}(\cdot), \quad \lambda_j \sim \pi_{\text{local}}(\cdot).$$

For interested readers, a full description of the data and model can be found in Nishimura and Suchard (2022).

We compare variations of the Gibbs samplers differing only in their conditional updates of the regression coefficients. Directly sampling from the conditional distribution of β is expensive due to ill-conditioning, so all samplers draw from the preconditioned scale with $\tilde{\beta}_j = \beta_j / (\tau \lambda_j)$ (Nishimura and Suchard, 2022), which has the following log-concave density:

$$\tilde{\beta} \mid y, X, \tau, \lambda \propto \left\{ \prod_i p_i(\tilde{\beta})^{y_i} [1 - p_i(\tilde{\beta})]^{1-y_i} \right\} e^{-\tilde{\beta}^\top \tilde{\beta} / 2}$$

This conditional update is traditionally dealt with using the Pólya–Gamma augmentation of Polson et al. (2013), conditioning on the additional parameter ω so that the distribution $\beta \mid y, X, \omega, \tau, \lambda$ becomes Gaussian. We run this augmented Gibbs sampler as a baseline comparison. The BPS and its bouncy Hamiltonian counterpart forego the augmentation and sample directly from the log-concave distribution.

The samplers are started from the same initial position at stationarity, determined by running 4,000 iterations of the Pólya–Gamma augmented sampler and taking the final sample. With the tuning strategy described in Section 5.1, the base step size for the No-U-Turn HBPS was derived to be 0.1, and optimal travel time for the standard version to be 1.5. The BPS also requires selecting a travel time and, additionally, a refresh rate. We conduct a grid search over both parameters. We start the travel time at 1.5 as chosen for the HBPS and adjust it by increments of ± 0.5 . We start with a refresh rate of 1 as suggested in Deligiannidis et al. (2021) for standard normal distributions and adjust it by increments of ± 0.2 . This approach finds the optimal refreshment rate to be 0.2, the lower boundary of the initial search grid. We thus refine our search grid on the lower end so

Table 1: Relative ESS per time across all regression coefficients for the sparse logistic model. The values are relative to the BPS.

	Relative ESS per time
Pólya–Gamma	0.36
BPS	1
HBPS with No-U-Turn	1.29
HBPS	4.02

that optimal parameters are within the boundaries of the new grid. Specifically, we add 0.1, 0.05, 0.01, and 0.005 to the new search grid, confirming that a refresh rate of 0.005 is not the best performing choice. For the BPS, a travel time of 1.5 is optimal along with a refresh rate of 0.01, with performance being much more sensitive to travel time choice than refresh rate.

We present results in Table 1. All samplers achieved at least 60 effective samples for each dimension. While results are presented in terms of relative efficiency to facilitate comparison, we note the computational challenge involved in this large-scale application, where the raw ESS per hour of the tuned BPS is 0.45. Each run takes approximately a week to complete, and over 14,000 hours of total CPU time were required to tune and generate the final comparison.

In our simulations, the standard tuned HBPS is the best performing sampler by a factor of four over the BPS. The No-U-Turn version is less efficient due its paths requiring more computation time, but it remains superior to the BPS under any tuning parameter (Figure 2). The competitive performance and minimal tuning requirement makes this an attractive option for practical purposes.

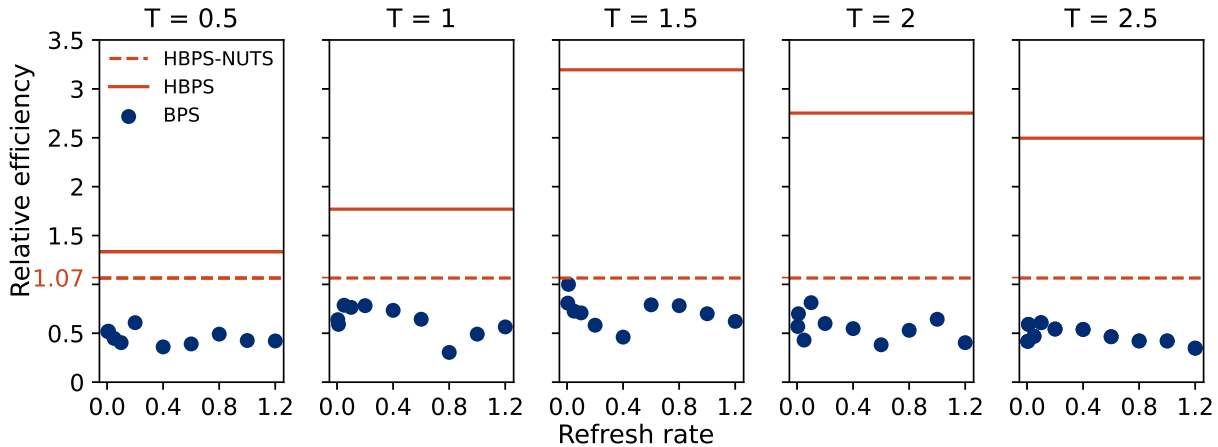


Figure 2: Comparison of the HBPS with No-U-Turn (red dashed) and without (red solid), along with the BPS (blue points) under the five best travel time parameters and a variety of refresh rates for the model in Section 5.2. Results are presented in terms of efficiency relative to the single best run of the BPS.

The Pólya–Gamma augmented sampler is the slowest performing sampler overall. When dealing with binomial outcomes more generally, the Pólya–Gamma sampler is known to suffer from poor mixing if the outcomes are imbalanced (Johndrow et al., 2019). HBPS’s ability to forego the data augmentation and directly target the log-concave conditional is therefore likely to provide an even greater advantage when dealing with imbalanced binomial outcomes.

5.3 Phylogenetic probit model: conditionally truncated Gaussian and splitting for joint update

Our second target comes from a model that quantifies the biological covariation among binary traits for the HIV virus while accounting for spurious correlations from shared evolutionary history. Of scientific interest is identifying which mutations are associated with immune response and viral virulence. To investigate this, Zhang et al. (2021) employ

a Bayesian phylogenetic probit model. We provide a brief summary of the data and model below, and refer readers to Zhang et al. (2021) for further details.

The data consist of $n = 535$ HIV viruses, each with $m = 21$ traits, collected from patients in Botswana and South Africa (Payne et al., 2014). The model uses continuous latent biological traits $x \in \mathbb{R}^{m \times n}$ which follow a phylogenetic Brownian diffusion parametrized by a phylogenetic tree \mathcal{T} and diffusion covariance $\Gamma \in \mathbb{R}^{m \times m}$. The observed binary outcomes $y = \text{sign}(x) \in \mathbb{R}^{m \times n}$ indicate the presence of traits in each virus. The primary parameter of interest is the covariance matrix Γ , which represents biological covariation independent of phylogenetic history among the m binary traits. The across-trait correlation and partial correlation matrices give insight into potential causal pathways from mutations to disease security and infectiousness of viruses.

The inference relies on a Gibbs scheme applied to the joint posterior (x, Γ, \mathcal{T}) , whose bottleneck is updating from the conditional $x \mid \Gamma, \mathcal{T}, y$. As in the application of the previous section, we vary the choice of sampler for this conditional update. This conditional follows a $535 \times 21 = 11,235$ dimensional truncated normal distribution of the form:

$$x \mid \Gamma, \mathcal{T}, y \sim N\{\mu(\Gamma, \mathcal{T}), \Sigma(\Gamma, \mathcal{T})\} \text{ truncated to } \{\text{sign}(x) = y\}.$$

Special features of this posterior make the HBPS an attractive choice of sampler. The covariance matrix of $\Sigma(\Gamma, \mathcal{T})$ depends on the other parameter values, and hence changes during each scan of the Gibbs sampler. This makes exact sampling with HMC (Pakman and Paninski, 2014) prohibitively expensive, requiring a 11,235 dimensional matrix inverse each iteration to simulate Hamiltonian dynamics. On the other hand, the dynamic programming trick of Zhang et al. (2021) allows us to compute matrix-vector multiplications by the precision matrix in $O(np^2)$ time instead of the usual $O(n^2p^2)$. Both BPS and HBPS rely only on this operation for their implementation. Another feature is the

high correlation between the two parameters x and Γ which leads to slower mixing when updating them conditionally (Liu, 2001). The deterministic and reversible nature of the HBPS dynamics allows for a joint update via an operator splitting scheme (Nishimura et al., 2020; Shahbaba et al., 2014). The splitting scheme approximates the *joint dynamics* on x, Γ for time Δt via a scheme similar to Section 2.2.2 of Zhang et al. (2022): we first simulate the dynamics of Γ given the initial value of x for a half step $\Delta t/2$, then simulate the dynamics of x given the updated Γ for a full step Δt , and finally simulate Γ given the final position of x for a half step $\Delta t/2$.

Zhang et al. (2022) update x conditionally on Γ using the BPS, which we replicate as a baseline using the same parameters. For comparison, we run two Gibbs samplers utilizing the HBPS. The first simply updates x with the HBPS and a tuned travel time of 1. The second uses the joint update of the Γ and x with operator splitting, with the number of steps taken decided by the No-U-Turn algorithm. For all the samplers and both conditional and joint updates, sampling of Γ relies on the Gaussian momentum based Hamiltonian dynamics with leapfrog approximation. Ten percent of the samples from all methods are discarded as burn in.

We measure minimum ESS across all unique elements of the correlation and partial correlation matrices and normalize by computation time, ensuring all samplers achieved a minimum of 100 effective samples. Final results are averaged over five runs with different seeds, and are presented in Table 2 relative to the performance of the BPS. Like the sparse logistic regression example in Section 5.2, the scale of the data necessitates multiple days of computation for each sampler, with the BPS achieving an average raw ESS per hour of 3.9.

For the correlation parameters, all samplers exhibit similar performance. However,

Table 2: Relative ESS per time across all unique elements of correlation and partial correlation matrices for the phylogenetic model.

	relative ESS per time	
	correlation	partial correlation
BPS	1	1
HBPS	1.32	0.91
HBPS with splitting and No-U-Turn	1.28	2.81

differences are evident for the partial correlation parameters, which Zhang et al. (2022) consider more difficult to sample from. Compared to the BPS, the standard HBPS is about equivalent, while the operator splitting approach achieves a 2.8 times speedup.

We note that the data subsampling approach popular in the PDMP literature is not applicable here since the phylogenetic model grows in dimension as the number of observations grows, so there is no redundancy in the data.

6 Discussion

In this article, we have presented a framework that unifies two of the most important paradigms in Bayesian computation. Our bouncy Hamiltonian dynamics use deterministic bounces to both generalize Hamiltonian dynamics and connect it to PDMPs through an inertia refreshment limit. We now present two techniques to further generalize bouncy Hamiltonian dynamics and broaden its practical applicability.

6.1 Numerical approximation of bouncy Hamiltonian dynamics

In some situations, surrogate dynamics or bounce times cannot be solved for exactly. The former can occur, for example, if the chosen surrogate potential is not trivial, and the latter if the target is not log-concave. While this article demonstrated bouncy Hamiltonian dynamics on examples admitting exact simulations, we now present a numerical approximation scheme based on the splitting technique (Strang, 1968; McLachlan and Quispel, 2002) to extend the algorithm’s scope to more general targets. While splitting is widely used for numerically solving differential equations, our scheme is unique in its ability to approximate bouncy dynamics that combine surrogate dynamics with a discontinuous bounce mechanism, and is partially inspired by the splitting scheme of Bertazzi et al. (2023) for PDMPs. Outlined in Algorithm 3, our deterministic scheme can be constructed from either an exact solution operator Φ of the surrogate dynamics or approximate one $\hat{\Phi}$ based, for example, on the leapfrog integrator. Algorithm 3 is time-reversible and volume preserving whenever Φ or $\hat{\Phi}$, if used, is time-reversible and volume preserving, and hence generates valid Metropolis proposals. The scheme starts by taking a half step in the position and velocity. It then updates the inertia with a midpoint approximation

$$U_{\text{dif}}(x_{\Delta t}) - U_{\text{dif}}(x_0) = \int_0^{\Delta t} v_s^\top \nabla U_{\text{dif}}(x_s) \, ds \approx \Delta t v_{\Delta t/2}^\top \nabla U_{\text{dif}}(x_{\Delta t/2})$$

if the trajectory has sufficient inertia for the half step or reflects the velocity otherwise. It completes the cycle by making the remaining half step. When using this approximate bouncy dynamics, generated proposals are no longer rejection-free and hence Algorithm 2 must be modified to include a Metropolis acceptance-rejection to ensure the correction stationary distribution.

Algorithm 3 Bouncy Hamiltonian dynamics numerical integrator for step Δt .

$$x_{\Delta t/2}, v_{\Delta t/2} \leftarrow \Phi(\Delta t/2, x_0, v_0) \text{ or } \hat{\Phi}(\Delta t/2, x_0, v_0)$$

$$l' \leftarrow l_0 - \Delta t \nabla U_{\text{dif}}(x_{\Delta t/2})^\top v_{\Delta t/2}$$

if $l' > 0$ **then**

$$l_{\Delta t} \leftarrow l'$$

else

$$l_{\Delta t} \leftarrow l_0$$

$$v_{\Delta t/2} \leftarrow R_{x_{\Delta t/2}}(v_{\Delta t/2})$$

end if

$$x_{\Delta t}, v_{\Delta t} \leftarrow \Phi(\Delta t/2, x_{\Delta t/2}, v_{\Delta t/2}) \text{ or } \hat{\Phi}(\Delta t/2, x_{\Delta t/2}, v_{\Delta t/2})$$

6.2 Local bouncy Hamiltonian dynamics

Our bouncy Hamiltonian dynamics can be generalized in a manner akin to local methods described in Section 3 of Bouchard-Côté et al. (2018) and Section 2.2.2 of Vanetti et al. (2017). These methods are applicable when the target density can be represented as a product

$$\pi(x) \propto \prod_{f=1}^F \gamma_f(x)$$

where γ_f is referred to as a *factor* and depends only on the subset of the coordinates of x indexed by $N_f \subseteq \{1, \dots, d\}$. In this case, the potential energy becomes a sum

$$U(x) = \sum_{f=1}^F U_f(x)$$

where $U_f = -\log \gamma_f$ has the property that $\partial U_f(x)/\partial x_k = 0$ for all $k \notin N_f$. For a local PDMP, each factor has its own event rate $\lambda_f = v^\top \nabla U_f$, and the first factor to experience a bounce event causes a corresponding change in velocity. The bounce occurs against ∇U_f

and affects v_k for $k \in N_f$ according to the restricted reflection function:

$$R_x(v, f) = v - 2 \frac{v^\top \nabla U_f(x)}{\|\nabla U_f(x)\|^2} \nabla U_f(x).$$

These local schemes provide opportunities to efficiently compute event times in applications such as factor graph models (Bouchard-Côté et al., 2018).

We now adapt this localization idea to bouncy Hamiltonian dynamics. Instead of a Poisson process, we associate an inertia $l_{f,0} \sim \text{Exp}(1)$ to each factor. These inertias evolve according to a local analogue of Equation (11):

$$l_{f,t} = l_{f,0} - \int_0^t v_s^\top \nabla U_f(x_s) ds.$$

For each factor, we can compute the time when inertia runs out as

$$t_f^* = \inf_{t>0} \left\{ l_{f,0} = \int_0^t v_s^\top \nabla U_f(x_s) ds \right\}.$$

The bounces occurs at time $\min_f t_f^*$, following the same restricted reflection function as in the local PDMP. The process is then repeated with this new velocity.

A special case of the local bouncy Hamiltonian dynamics is when the factors partition the parameter space. With a single factor $N_1 = \{1, \dots, d\}$, we recover the standard bouncy Hamiltonian dynamics. With d coordinate-wise factors $N_i = \{i\}$ and a constant surrogate potential, we get the Hamiltonian zig-zag sampler of Nishimura et al. (2024).

Local bouncy Hamiltonian dynamics retains the same properties outlined in Theorem 1, with the proof almost identical to the standard case, and thus generates valid Metropolis proposals. Analogues of Theorems 2 and 3 also hold, connecting local bouncy Hamiltonian dynamics to local PDMPs: when combined with periodic refreshments of each factor's inertia, the dynamics converge to the local PDMPs in the limit.

References

- Alder, B. J. and Wainwright, T. E. (1959). Studies in molecular dynamics. i. general method. *The Journal of Chemical Physics*, 31(2):459–466.
- Bertazzi, A., Dobson, P., and Monmarché, P. (2023). Splitting schemes for second order approximations of piecewise-deterministic Markov processes. *arXiv preprint arXiv:2301.02537*.
- Bierkens, J., Bouchard-Côté, A., Doucet, A., Duncan, A. B., Fearnhead, P., Lienart, T., Roberts, G., and Vollmer, S. J. (2018). Piecewise deterministic Markov processes for scalable Monte carlo on restricted domains. *Statistics & Probability Letters*, 136:148–154.
- Bierkens, J., Fearnhead, P., and Roberts, G. (2019). The Zig-Zag process and super-efficient sampling for Bayesian analysis of big data. *The Annals of Statistics*, 47(3):1288 – 1320.
- Bierkens, J., Grazi, S., Kamatani, K., and Roberts, G. (2020). The boomerang sampler. In *International conference on machine learning*, pages 908–918. PMLR.
- Billingsley, P. (1999). *Convergence of probability measures*. Wiley Series in Probability and Statistics: Probability and Statistics. John Wiley & Sons Inc., New York, second edition.
- Blanes, S., Casas, F., and Sanz-Serna, J. M. (2014). Numerical integrators for the hybrid Monte Carlo method. *SIAM Journal on Scientific Computing*, 36(4):A1556–A1580.
- Bou-Rabee, N. and Sanz-Serna, J. M. (2017). Randomized Hamiltonian Monte Carlo. *The Annals of Applied Probability*, 27(4):2159–2194.
- Bou-Rabee, N. and Sanz-Serna, J. M. (2018). Geometric integrators and the Hamiltonian Monte Carlo method. *Acta Numerica*, 27:113–206.

- Bouchard-Côté, A., Vollmer, S. J., and Doucet, A. (2018). The bouncy particle sampler: A nonreversible rejection-free Markov chain Monte Carlo method. *Journal of the American Statistical Association*, 113(522):855–867.
- Carpenter, B., Gelman, A., Hoffman, M. D., Lee, D., Goodrich, B., Betancourt, M., Brubaker, M., Guo, J., Li, P., and Riddell, A. (2017). Stan: A probabilistic programming language. *Journal of statistical software*, 76(1).
- Davis, M. H. (1984). Piecewise-deterministic Markov processes: A general class of non-diffusion stochastic models. *Journal of the Royal Statistical Society: Series B (Methodological)*, 46(3):353–376.
- Deligiannidis, G., Paulin, D., Bouchard-Côté, A., and Doucet, A. (2021). Randomized Hamiltonian Monte Carlo as scaling limit of the bouncy particle sampler and dimension-free convergence rates. *The Annals of Applied Probability*, 31(6):2612–2662.
- Diaconis, P., Holmes, S., and Neal, R. M. (2000). Analysis of a nonreversible Markov chain sampler. *Annals of Applied Probability*, pages 726–752.
- Duane, S., Kennedy, A. D., Pendleton, B. J., and Roweth, D. (1987). Hybrid Monte Carlo. *Physics letters B*, 195(2):216–222.
- Dunson, D. B. and Johndrow, J. E. (2020). The Hastings algorithm at fifty. *Biometrika*, 107(1):1–23.
- Ethier, S. N. and Kurtz, T. G. (2009). *Markov processes: characterization and convergence*. John Wiley & Sons.
- Fang, Y., Sanz-Serna, J.-M., and Skeel, R. D. (2014). Compressible generalized hybrid Monte Carlo. *The Journal of chemical physics*, 140(17):174108.

- Fearnhead, P., Bierkens, J., Pollock, M., and Roberts, G. O. (2018). Piecewise deterministic Markov processes for continuous-time Monte Carlo. *Statistical Science*, 33(3):386–412.
- Girolami, M. and Calderhead, B. (2011). Riemann manifold Langevin and Hamiltonian Monte Carlo methods. *Journal of the Royal Statistical Society Series B: Statistical Methodology*, 73(2):123–214.
- Gustafson, P. (1998). A guided walk Metropolis algorithm. *Statistics and computing*, 8:357–364.
- Hoffman, M. D., Gelman, A., et al. (2014). The no-u-turn sampler: adaptively setting path lengths in Hamiltonian Monte Carlo. *J. Mach. Learn. Res.*, 15(1):1593–1623.
- Johndrow, J. E., Smith, A., Pillai, N., and Dunson, D. B. (2019). MCMC for imbalanced categorical data. *Journal of the American Statistical Association*, 114(527):1394–1403.
- Liu, J. S. (2001). *Monte Carlo strategies in scientific computing*, volume 75. Springer.
- Livingstone, S., Betancourt, M., Byrne, S., and Girolami, M. (2019a). On the geometric ergodicity of Hamiltonian Monte Carlo. *Bernoulli*, 25(4A):3109 – 3138.
- Livingstone, S., Faulkner, M. F., and Roberts, G. O. (2019b). Kinetic energy choice in Hamiltonian/hybrid Monte Carlo. *Biometrika*, 106(2):303–319.
- McLachlan, R. I. and Quispel, G. R. W. (2002). Splitting methods. *Acta Numerica*, 11:341–434.
- Metropolis, N., Rosenbluth, A. W., Rosenbluth, M. N., Teller, A. H., and Teller, E. (1953). Equation of state calculations by fast computing machines. *The journal of chemical physics*, 21(6):1087–1092.

- Mira, A. et al. (2001). On Metropolis-Hastings algorithms with delayed rejection. *Metron*, 59(3-4):231–241.
- Neal, R. M. et al. (2011). MCMC using Hamiltonian dynamics. *Handbook of markov chain monte carlo*, 2(11):2.
- Nishimura, A., Dunson, D. B., and Lu, J. (2020). Discontinuous Hamiltonian Monte Carlo for discrete parameters and discontinuous likelihoods. *Biometrika*, 107(2):365–380.
- Nishimura, A. and Suchard, M. A. (2022). Prior-preconditioned conjugate gradient method for accelerated Gibbs sampling in “large n, large p” Bayesian sparse regression. *Journal of the American Statistical Association*, pages 1–14.
- Nishimura, A., Zhang, Z., and Suchard, M. A. (2024). Zigzag path connects two Monte Carlo samplers: Hamiltonian counterpart to a piecewise deterministic Markov process. *arXiv preprint arXiv:2104.07694*.
- Pakman, A. and Paninski, L. (2014). Exact Hamiltonian Monte Carlo for truncated multivariate gaussians. *Journal of Computational and Graphical Statistics*, 23(2):518–542.
- Payne, R., Muenchhoff, M., Mann, J., Roberts, H. E., Matthews, P., Adland, E., Hempenstall, A., Huang, K.-H., Brockman, M., Brumme, Z., et al. (2014). Impact of HLA-driven HIV adaptation on virulence in populations of high HIV seroprevalence. *Proceedings of the National Academy of Sciences*, 111(50):E5393–E5400.
- Peters, E. A. et al. (2012). Rejection-free Monte Carlo sampling for general potentials. *Physical Review E*, 85(2):026703.
- Plummer, M., Best, N., Cowles, K., Vines, K., et al. (2006). CODA: convergence diagnosis and output analysis for MCMC. *R news*, 6(1):7–11.

- Polson, N. G., Scott, J. G., and Windle, J. (2013). Bayesian inference for logistic models using Pólya–gamma latent variables. *Journal of the American statistical Association*, 108(504):1339–1349.
- Rosenbaum, P. R. and Rubin, D. B. (1983). The central role of the propensity score in observational studies for causal effects. *Biometrika*, 70(1):41–55.
- Salvatier, J., Wiecki, T. V., and Fonnesbeck, C. (2016). Probabilistic programming in Python using PyMC3. *PeerJ Computer Science*, 2:e55.
- Shahbaba, B., Lan, S., Johnson, W. O., and Neal, R. M. (2014). Split Hamiltonian Monte Carlo. *Statistics and Computing*, 24:339–349.
- Sherlock, C. and Thiery, A. H. (2022). A discrete bouncy particle sampler. *Biometrika*, 109(2):335–349.
- Strang, G. (1968). On the construction and comparison of difference schemes. *SIAM journal on numerical analysis*, 5(3):506–517.
- Tian, Y., Schuemie, M. J., and Suchard, M. A. (2018). Evaluating large-scale propensity score performance through real-world and synthetic data experiments. *International Journal of Epidemiology*.
- Vanetti, P., Bouchard-Côté, A., Deligiannidis, G., and Doucet, A. (2017). Piecewise-deterministic Markov chain Monte Carlo. *arXiv preprint arXiv:1707.05296*.
- Wright, S., Nocedal, J., et al. (1999). Numerical optimization. *Springer Science*, 35(67-68):7.
- Zhang, Z., Nishimura, A., Bastide, P., Ji, X., Payne, R. P., Goulder, P., Lemey, P., and Suchard, M. A. (2021). Large-scale inference of correlation among mixed-type biological

traits with phylogenetic multivariate probit models. *The Annals of Applied Statistics*, 15(1):230 – 251.

Zhang, Z., Nishimura, A., Trovão, N. S., Cherry, J. L., Holbrook, A. J., Ji, X., Lemey, P., and Suchard, M. A. (2022). Accelerating Bayesian inference of dependency between complex biological traits. *arXiv preprint arXiv:2201.07291*.

Supplement for “MCMC using *bouncy* Hamiltonian dynamics: A unifying framework for Hamiltonian Monte Carlo and piecewise deterministic Markov process samplers”

Andrew Chin

Department of Biostatistics, Bloomberg School of Public Health,
Johns Hopkins University

and

Akihiko Nishimura

Department of Biostatistics, Bloomberg School of Public Health,
Johns Hopkins University

May 15, 2024

1 Proof of Theorem 1

The proof that the dynamics must start away from a measure 0 set follows from a nearly identical argument to Supplement S1 of Nishimura et al. (2024) and is omitted for brevity. Staying away from this set of vanishing gradient ensures the dynamics are well defined. If the inertia were to run out exactly at a point where $\nabla U_{\text{sur}}(x) = 0$, the bounce direction is indeterminate.

For any dynamics with solution operator $\Phi(T, x_0, v_0, l_0)$ that returns the state at time T , denoted (x_T, v_T, l_T) , time-reversibility is the property that $(x_0, v_0, l_0) = \Phi(T, x_T, -v_T, l_T)$. That is, by reversing the velocity alone, we can recover the initial state by simulating the dynamics for another T duration. Volume-preservation is defined as the Jacobian of the

mapping $(x_0, v_0, l_0) \mapsto (x_T, v_T, l_T)$ having absolute determinant one.

Time reversibility follows from the fact that the underlying position-velocity dynamics is assumed to be reversible and the inertia evolution and the reflection process are trivially reversible. We are left to show conservation of the joint density and volume preservation.

Proof of conservation of augmented energy. Consider the negative log density of the joint distribution $-\log \pi(x, v, l) = -\log \pi(x) - \log \pi(v) - \log \pi(l)$, which is conserved if and only if the joint distribution is also conserved. Since $\pi(v)$ is symmetric in all directions, bounce events do not change the joint density, and so it suffices to show that the density is constant along the paths between the bounces. Crucially, the evolution of the inertia is constructed deliberately to counteract changes in $\pi(x)$ as the position changes, leading to the total density at any point to be independent of time. This is formalized as follows:

$$\begin{aligned}
\frac{\partial}{\partial t}[-\log \pi(x) - \log \pi(v) - \log \pi(l)] &= \frac{\partial}{\partial t}[U_{\text{tar}}(x_t) + K(v_t) + l_t] \\
&= \frac{\partial}{\partial t}[U_{\text{tar}}(x_t) + K(v_t) + l_0 + U_{\text{dif}}(x_0) - U_{\text{dif}}(x_t)] \\
&= \frac{\partial}{\partial t}[U_{\text{tar}}(x_t) + K(v_t) - U_{\text{dif}}(x_t)] \\
&= \frac{\partial}{\partial t}[U_{\text{tar}}(x_t) + K(v_t) - (U_{\text{tar}}(x_t) - U_{\text{sur}}(x_t))] \\
&= \frac{\partial}{\partial t}[K(v_t) + U_{\text{sur}}(x_t)] \\
&= 0,
\end{aligned}$$

where the last equality follows from the fact that the surrogate dynamics is energy conserving.

□

Proof of volume preservation. Without loss of generality, we can assume that at most one bounce occurs in the interval $[0, T]$, since composition of volume preserving maps is still volume preserving.

In the no bounce case, the $2d+1$ dimensional Jacobian J will be as follows, corresponding to the dynamics given solely by the surrogate dynamics. We let 0 and I represent the all zeros and identity matrix of appropriate dimension, respectively.

$$\begin{aligned}
J &= \begin{bmatrix} \frac{\partial x_T}{\partial x_0} & \frac{\partial x_T}{\partial v_0} & \frac{\partial x_T}{\partial l_0} \\ \frac{\partial v_T}{\partial x_0} & \frac{\partial v_T}{\partial v_0} & \frac{\partial v_T}{\partial l_0} \\ \frac{\partial l_T}{\partial x_0} & \frac{\partial l_T}{\partial v_0} & \frac{\partial l_T}{\partial l_0} \end{bmatrix} \\
&= \begin{bmatrix} \frac{\partial x_T}{\partial x_0} & \frac{\partial x_T}{\partial v_0} & 0 \\ \frac{\partial v_T}{\partial x_0} & \frac{\partial v_T}{\partial v_0} & 0 \\ \frac{\partial l_T}{\partial x_0} & \frac{\partial l_T}{\partial v_0} & 1 \end{bmatrix}.
\end{aligned}$$

By assumption, we have that

$$\det \begin{bmatrix} \frac{\partial x_T}{\partial x_0} & \frac{\partial x_T}{\partial v_0} \\ \frac{\partial v_T}{\partial x_0} & \frac{\partial v_T}{\partial v_0} \end{bmatrix} = 1.$$

The result then follows directly from the matrix identity

$$\det \begin{bmatrix} A & 0 \\ C & D \end{bmatrix} = \det A \det D.$$

Now consider the case where one bounce occurs at time t^* . Let $\Phi_l(t, x, v, l) : \mathbb{R}^{2d+1} \rightarrow \mathbb{R}^{2d+1}$ denote the solution operator of the bouncy Hamiltonian dynamics *without any bounces*, which takes an initial state x, v, l and duration t and returns (x_t, v_t, l_t) , the state after the dynamics is simulated for time t . Because no bounces are considered in Φ_l , the full dynamics *with* a bounce at time t^* can be represented as

$$\Phi_l(T - t^*, R \circ \Phi_l(t^*, z_0)),$$

which we now show has Jacobian with absolute determinant one. First we write the Jacobian as follows:

$$\begin{aligned}
J &= \frac{d}{dz_0} \Phi_l \{ T - t^*, R \circ \Phi_l(t^*, z_0) \} \\
&= - \frac{\partial \Phi_l}{\partial t} \Big|_{t=T-t^*, z=R \circ \Phi_l(t^*, z_0)} \frac{\partial t^*}{\partial z_0} + \frac{\partial \Phi_l}{\partial z} \Big|_{t=T-t^*, z=R \circ \Phi_l(t^*, z_0)} \frac{\partial(R \circ \Phi_l(t^*, z))}{\partial z} \Big|_{t=t^*, z=z_0} \\
&= - \frac{\partial \Phi_l}{\partial t} \Big|_{t=T-t^*, z=R \circ \Phi_l(t^*, z_0)} \frac{\partial t^*}{\partial z_0} \\
&\quad + \frac{\partial \Phi_l}{\partial z} \Big|_{t=T-t^*, z=R \circ \Phi_l(t^*, z_0)} \left(\frac{\partial(R \circ \Phi_l)}{\partial t} \Big|_{t=t^*, z=z_0} \frac{\partial t^*}{\partial z_0} + \frac{\partial(R \circ \Phi_l)}{\partial z} \Big|_{t=t^*, z=z_0} \right) \\
&= - \frac{\partial \Phi_l}{\partial t} \Big|_{t=T-t^*, z=R \circ \Phi_l(t^*, z_0)} \frac{\partial t^*}{\partial z_0} \\
&\quad + \frac{\partial \Phi_l}{\partial z} \Big|_{t=T-t^*, z=R \circ \Phi_l(t^*, z_0)} \frac{\partial(R \circ \Phi_l)}{\partial t} \Big|_{t=t^*, z=z_0} \frac{\partial t^*}{\partial z_0} \\
&\quad + \frac{\partial \Phi_l}{\partial z} \Big|_{t=T-t^*, z=R \circ \Phi_l(t^*, z_0)} \frac{\partial(R \circ \Phi_l)}{\partial z} \Big|_{t=t^*, z=z_0} \\
&= \left(- \frac{\partial \Phi_l}{\partial t} \Big|_{t=T-t^*, z=R \circ \Phi_l(t^*, z_0)} + \frac{\partial \Phi_l}{\partial z} \Big|_{t=T-t^*, z=R \circ \Phi_l(t^*, z_0)} \frac{\partial(R \circ \Phi_l)}{\partial t} \Big|_{t=t^*, z=z_0} \right) \frac{\partial t^*}{\partial z_0} \\
&\quad + \frac{\partial \Phi_l}{\partial z} \Big|_{t=T-t^*, z=R \circ \Phi_l(t^*, z_0)} \frac{\partial(R \circ \Phi_l)}{\partial z} \Big|_{t=t^*, z=z_0} \\
&= \left(- \frac{\partial \Phi_l}{\partial t} \Big|_{t=T-t^*, z=R \circ \Phi_l(t^*, z_0)} + \frac{\partial \Phi_l}{\partial z} \Big|_{t=T-t^*, z=R \circ \Phi_l(t^*, z_0)} \frac{\partial R}{\partial z} \Big|_{z=\Phi_l(t^*, z_0)} \frac{\partial \Phi_l}{\partial t} \Big|_{t=t^*, z=z_0} \right) \frac{\partial t^*}{\partial z_0} \\
&\quad + \frac{\partial \Phi_l}{\partial z} \Big|_{t=T-t^*, z=R \circ \Phi_l(t^*, z_0)} \frac{\partial R}{\partial z} \Big|_{z=\Phi_l(t^*, z_0)} \frac{\partial \Phi_l}{\partial z} \Big|_{t=t^*, z=z_0}.
\end{aligned}$$

By the matrix determinant lemma, we have that

$$\det(J) = (1 + w^\top M^{-1}u) \det(M),$$

where

$$\begin{aligned}
M &= \frac{\partial \Phi_l}{\partial z} \Big|_{t=T-t^*, z=R \circ \Phi_l(t^*, z_0)} \frac{\partial R}{\partial z} \Big|_{z=\Phi_l(t^*, z_0)} \frac{\partial \Phi_l}{\partial z} \Big|_{t=t^*, z=z_0} \\
w^\top &= \frac{\partial t^*}{\partial z_0} \\
u &= - \frac{\partial \Phi_l}{\partial t} \Big|_{t=T-t^*, z=R \circ \Phi_l(t^*, z_0)} + \frac{\partial \Phi_l}{\partial z} \Big|_{t=T-t^*, z=R \circ \Phi_l(t^*, z_0)} \frac{\partial R}{\partial z} \Big|_{z=\Phi_l(t^*, z_0)} \frac{\partial \Phi_l}{\partial t} \Big|_{t=t^*, z=z_0}.
\end{aligned}$$

$|\det M| = 1$ because the reflection function has determinant -1 and we have shown Φ_l is volume preserving.

To show $|\det J| = 1$, it then suffices to show $w^\top M^{-1}u = -2$. First we rearrange the terms:

$$\begin{aligned}
w^\top M^{-1}u &= \frac{\partial t^*}{\partial z_0} \\
&\times \left(\frac{\partial \Phi_l}{\partial z} \Big|_{t=T-t^*, z=R \circ \Phi_l(t^*, z_0)} \quad \frac{\partial R}{\partial z} \Big|_{z=\Phi_l(t^*, z_0)} \quad \frac{\partial \Phi_l}{\partial z} \Big|_{t=t^*, z=z_0} \right)^{-1} \\
&\times \left(-\frac{\partial \Phi_l}{\partial t} \Big|_{t=T-t^*, z=R \circ \Phi_l(t^*, z_0)} \right. \\
&\quad \left. + \frac{\partial \Phi_l}{\partial z} \Big|_{t=T-t^*, z=R \circ \Phi_l(t^*, z_0)} \quad \frac{\partial R}{\partial z} \Big|_{z=\Phi_l(t^*, z_0)} \quad \frac{\partial \Phi_l}{\partial t} \Big|_{t=t^*, z=z_0} \right) \\
&= \frac{\partial t^*}{\partial z_0} \\
&\times \frac{\partial \Phi_l}{\partial z} \Big|_{t=t^*, z=z_0}^{-1} \quad \frac{\partial R}{\partial z} \Big|_{z=\Phi_l(t^*, z_0)}^{-1} \quad \frac{\partial \Phi_l}{\partial z} \Big|_{t=T-t^*, z=R \circ \Phi_l(t^*, z_0)}^{-1} \\
&\times \left(-\frac{\partial \Phi_l}{\partial t} \Big|_{t=T-t^*, z=R \circ \Phi_l(t^*, z_0)} \right. \\
&\quad \left. + \frac{\partial \Phi_l}{\partial z} \Big|_{t=T-t^*, z=R \circ \Phi_l(t^*, z_0)} \quad \frac{\partial R}{\partial z} \Big|_{z=\Phi_l(t^*, z_0)} \quad \frac{\partial \Phi_l}{\partial t} \Big|_{t=t^*, z=z_0} \right) \\
&= \frac{\partial t^*}{\partial z_0} \frac{\partial \Phi_l}{\partial z} \Big|_{t=t^*, z=z_0}^{-1} \\
&\times \left(\frac{\partial \Phi_l}{\partial t} \Big|_{t=t^*, z=z_0} \right. \\
&\quad \left. - \frac{\partial R}{\partial z} \Big|_{z=\Phi_l(t^*, z_0)}^{-1} \quad \frac{\partial \Phi_l}{\partial z} \Big|_{t=T-t^*, z=R \circ \Phi_l(t^*, z_0)}^{-1} \quad \frac{\partial \Phi_l}{\partial t} \Big|_{t=T-t^*, z=R \circ \Phi_l(t^*, z_0)} \right).
\end{aligned}$$

Consider the term

$$\frac{\partial t^*}{\partial z_0} \frac{\partial \Phi_l}{\partial z} \Big|_{t=t^*, z=z_0}^{-1}.$$

We write these as block matrices and use the identity

$$\begin{bmatrix} A & B \\ C & D \end{bmatrix}^{-1} = \begin{bmatrix} A^{-1} + A^{-1}B(D - CA^{-1}B)^{-1}CA^{-1} & -A^{-1}B(D - CA^{-1}B)^{-1} \\ -(D - CA^{-1}B)^{-1}CA^{-1} & (D - CA^{-1}B)^{-1} \end{bmatrix},$$

with A being the $2p \times 2p$ block in the top left:

$$\begin{aligned}
\left. \frac{\partial t^*}{\partial z_0} \frac{\partial \Phi_l}{\partial z} \right|_{t=t^*, z=z_0}^{-1} &= \left[\begin{array}{ccc} \frac{\partial t^*}{\partial x_0} & \frac{\partial t^*}{\partial v_0} & \frac{\partial t^*}{\partial l_0} \end{array} \right] \left[\begin{array}{ccc} \frac{\partial x}{\partial x_0} & \frac{\partial x}{\partial v_0} & \frac{\partial x}{\partial l_0} \\ \frac{\partial v}{\partial x_0} & \frac{\partial v}{\partial v_0} & \frac{\partial v}{\partial l_0} \\ \frac{\partial l}{\partial x_0} & \frac{\partial l}{\partial v_0} & \frac{\partial l}{\partial l_0} \end{array} \right] \Big|_{t=t^*, z=z_0}^{-1} \\
&= \left[\begin{array}{ccc} \frac{\partial t^*}{\partial x_0} & \frac{\partial t^*}{\partial v_0} & \frac{\partial t^*}{\partial l_0} \end{array} \right] \left[\begin{array}{cc} A & 0 \\ \left[\begin{array}{cc} \frac{\partial l}{\partial x_0} & \frac{\partial l}{\partial v_0} \end{array} \right] & 1 \end{array} \right] \Big|_{t=t^*, z=z_0}^{-1} \\
&= \left[\begin{array}{ccc} \frac{\partial t^*}{\partial x_0} & \frac{\partial t^*}{\partial v_0} & \frac{\partial t^*}{\partial l_0} \end{array} \right] \left[\begin{array}{cc} A^{-1} & 0 \\ - \left[\begin{array}{cc} \frac{\partial l}{\partial x_0} & \frac{\partial l}{\partial v_0} \end{array} \right] A^{-1} & 1 \end{array} \right] \Big|_{t=t^*, z=z_0} \\
&= \left[\left[\begin{array}{cc} \frac{\partial t^*}{\partial x_0} & \frac{\partial t^*}{\partial v_0} \end{array} \right] A^{-1} - \frac{\partial t^*}{\partial l_0} \left[\begin{array}{cc} \frac{\partial l}{\partial x_0} & \frac{\partial l}{\partial v_0} \end{array} \right] A^{-1} \quad \frac{\partial t^*}{\partial l_0} \right] \Big|_{t=t^*, z=z_0} \\
&= \left[\left(\left[\begin{array}{cc} \frac{\partial t^*}{\partial x_0} & \frac{\partial t^*}{\partial v_0} \end{array} \right] - \frac{\partial t^*}{\partial l_0} \left[\begin{array}{cc} \frac{\partial l}{\partial x_0} & \frac{\partial l}{\partial v_0} \end{array} \right] \right) A^{-1} \quad \frac{\partial t^*}{\partial l_0} \right] \Big|_{t=t^*, z=z_0} \\
&= \left[\left[\begin{array}{ccc} \frac{\partial t^*}{\partial x_0} & \frac{\partial t^*}{\partial l_0} \frac{\partial l}{\partial x_0} & \frac{\partial t^*}{\partial v_0} - \frac{\partial t^*}{\partial l_0} \frac{\partial l}{\partial v_0} \end{array} \right] A^{-1} \quad \frac{\partial t^*}{\partial l_0} \right] \Big|_{t=t^*, z=z_0}.
\end{aligned}$$

Define $f(t, x, v, l) = l - \int_0^t v_s^\top \nabla U_{\text{dif}}(x_s) ds$. Since $\partial f / \partial t = v_t^\top \nabla U_{\text{dif}}(x_t)$, as long as $v_t^\top \nabla U_{\text{dif}}(x_t) \neq 0$, the implicit function theorem (Spivak, 1965) allows us to implicitly differentiate t^* with respect to x_0, v_0 , and l_0 from the identity $l_0 = \int_0^{t^*} v_s^\top \nabla U_{\text{dif}}(x_s) ds$. Here $v_-^* = \lim_{t \uparrow t^*} v$ refers to the velocity before the reflection function is applied.

$$\begin{aligned}
\frac{\partial t^*}{\partial x_0} &= \frac{\nabla U_{\text{dif}}(x_0)^\top - \nabla U_{\text{dif}}(x^*)^\top \frac{\partial x^*}{\partial x_0}}{v_-^{*\top} \nabla U_{\text{dif}}(x^*)} \\
\frac{\partial t^*}{\partial v_0} &= - \frac{\nabla U_{\text{dif}}(x^*)^\top \frac{\partial x^*}{\partial v_0}}{v_-^{*\top} \nabla U_{\text{dif}}(x^*)} \\
\frac{\partial t^*}{\partial l_0} &= \frac{1}{v_-^{*\top} \nabla U_{\text{dif}}(x^*)}
\end{aligned}$$

By definition of the inertia dynamic, we also have:

$$\left. \frac{\partial l}{\partial x_0} \right|_{t=t^*, z=z_0} = \nabla U_{\text{dif}}(x_0) - \nabla U_{\text{dif}}(x^*) \frac{\partial x^*}{\partial x_0}, \quad \left. \frac{\partial l}{\partial v_0} \right|_{t=t^*, z=z_0} = -\nabla U_{\text{dif}}(x^*) \frac{\partial x^*}{\partial v_0}.$$

Plugging in, we get

$$\begin{aligned}
\left. \frac{\partial t^*}{\partial z_0} \frac{\partial \Phi_l}{\partial z} \right|_{t=t^*, z=z_0}^{-1} &= \left[\left[\frac{\partial t^*}{\partial x_0} - \frac{\partial t^*}{\partial l_0} \frac{\partial l}{\partial x_0} \quad \frac{\partial t^*}{\partial v_0} - \frac{\partial t^*}{\partial l_0} \frac{\partial l}{\partial v_0} \right] A^{-1} \frac{\partial t^*}{\partial l_0} \right] \Big|_{t=t^*, z=z_0} \\
&= \left[\begin{bmatrix} 0 & 0 \end{bmatrix} A^{-1} \frac{\partial t^*}{\partial l_0} \right] \\
&= \begin{bmatrix} 0 & \frac{\partial t^*}{\partial l_0} \end{bmatrix},
\end{aligned}$$

which is a vector of all 0's except for the final entry. Now we return to $w^\top M^{-1}u$:

$$\begin{aligned}
w^\top M^{-1}u &= \left. \frac{\partial t^*}{\partial z_0} \frac{\partial \Phi_l}{\partial z} \right|_{t=t^*, z=z_0}^{-1} \\
&\quad \times \left(\left. \frac{\partial \Phi_l}{\partial t} \right|_{t=t^*, z=z_0} \right. \\
&\quad \left. - \left. \frac{\partial R}{\partial z} \right|_{z=\Phi_l(t^*, z_0)}^{-1} \left. \frac{\partial \Phi_l}{\partial z} \right|_{t=T-t^*, z=R \circ \Phi_l(t^*, z_0)}^{-1} \left. \frac{\partial \Phi_l}{\partial t} \right|_{t=T-t^*, z=R \circ \Phi_l(t^*, z_0)} \right) \\
&= \begin{bmatrix} 0 & \frac{\partial t^*}{\partial l_0} \end{bmatrix} \left. \frac{\partial \Phi_l}{\partial t} \right|_{t=t^*, z=z_0} \\
&\quad - \begin{bmatrix} 0 & \frac{\partial t^*}{\partial l_0} \end{bmatrix} \left. \frac{\partial R}{\partial z} \right|_{z=\Phi_l(t^*, z_0)}^{-1} \left. \frac{\partial \Phi_l}{\partial z} \right|_{t=T-t^*, z=R \circ \Phi_l(t^*, z_0)}^{-1} \left. \frac{\partial \Phi_l}{\partial t} \right|_{t=T-t^*, z=R \circ \Phi_l(t^*, z_0)}.
\end{aligned}$$

For the first term in the sum, we have

$$\begin{aligned}
\begin{bmatrix} 0 & \frac{\partial t^*}{\partial l_0} \end{bmatrix} \left. \frac{\partial \Phi_l}{\partial t} \right|_{t=t^*, z=z_0} &= \frac{\partial t^*}{\partial l_0} \left. \frac{\partial l}{\partial t} \right|_{t=t^*, z=z_0} \\
&= \frac{1}{v_-^*{}^\top \nabla U_{\text{dif}}(x^*)} \left. \frac{\partial l}{\partial t} \right|_{t=t^*, z=z_0} \\
&= \frac{1}{v_-^*{}^\top \nabla U_{\text{dif}}(x^*)} \left(-\nabla U_{\text{dif}}(x^*)^\top \left. \frac{\partial x}{\partial t} \right|_{t=t^*, z=z_0} \right) \\
&= \frac{1}{v_-^*{}^\top \nabla U_{\text{dif}}(x^*)} (-\nabla U_{\text{dif}}(x^*)^\top v_-^*) \\
&= -1.
\end{aligned}$$

It remains to show the second term is 1. We can ignore $\frac{\partial R}{\partial z} \Big|_{z=\Phi_l(t^*, z_0)}^{-1}$ since

$$\frac{\partial R}{\partial z} \Big|_{z=\Phi_l(t^*, z_0)}^{-1} = \begin{bmatrix} \cdot & \cdot & \cdot \\ \cdot & \cdot & \cdot \\ 0 & 0 & 1 \end{bmatrix},$$

where the top two rows are not relevant because they will get multiplied by 0. Then,

$$\begin{aligned} & \begin{bmatrix} 0 & \frac{\partial t^*}{\partial l_0} \end{bmatrix} \frac{\partial R}{\partial z} \Big|_{z=\Phi_l(t^*, z_0)}^{-1} \frac{\partial \Phi_l}{\partial z} \Big|_{t=T-t^*, z=R \circ \Phi_l(t^*, z_0)}^{-1} \frac{\partial \Phi_l}{\partial t} \Big|_{t=T-t^*, z=R \circ \Phi_l(t^*, z_0)} \\ &= \begin{bmatrix} 0 & \frac{\partial t^*}{\partial l_0} \end{bmatrix} \frac{\partial \Phi_l}{\partial z} \Big|_{t=T-t^*, z=R \circ \Phi_l(t^*, z_0)}^{-1} \frac{\partial \Phi_l}{\partial t} \Big|_{t=T-t^*, z=R \circ \Phi_l(t^*, z_0)} \\ &= \begin{bmatrix} 0 & \frac{\partial t^*}{\partial l_0} \end{bmatrix} \frac{\partial \Phi_l^{-1}}{\partial z} \Big|_{t=T-t^*, z=z_T} \frac{\partial \Phi_l}{\partial t} \Big|_{t=T-t^*, z=R \circ \Phi_l(t^*, z_0)} \\ &= \frac{\partial t^*}{\partial l_0} \frac{\partial l^{-1}}{\partial z} \Big|_{t=T-t^*, z=z_T} \frac{\partial \Phi_l}{\partial t} \Big|_{t=T-t^*, z=R \circ \Phi_l(t^*, z_0)}. \end{aligned}$$

Now consider the following identity using inverse inertia function:

$$l^{-1}(T - t^*, z_T) = l^{-1}(T - t^* + s, \Phi_l(s, z_T)), \quad s \geq 0.$$

Since the left hand side is constant, taking derivative with respect to s yields:

$$\begin{aligned} 0 &= \frac{d}{ds} l^{-1}(T - t^* + s, \Phi_l(s, z_T)) \\ &= \frac{\partial l^{-1}}{\partial t} \Big|_{t=T-t^*+s, z=\Phi_l(s, z_T)} + \frac{\partial l^{-1}}{\partial z} \Big|_{t=T-t^*+s, z=\Phi_l(s, z_T)} \frac{\partial \Phi_l}{\partial t} \Big|_{t=s, z=z_T}. \end{aligned}$$

Since this holds for all $s \geq 0$, we set $s = 0$ and rearrange to get the following identity

$$\begin{aligned} - \frac{\partial l^{-1}}{\partial t} \Big|_{t=T-t^*, z=z_T} &= \frac{\partial l^{-1}}{\partial z} \Big|_{t=T-t^*, z=z_T} \frac{\partial \Phi_l}{\partial t} \Big|_{t=0, z=z_T} \\ &= \frac{\partial l^{-1}}{\partial z} \Big|_{t=T-t^*, z=z_T} \frac{\partial \Phi_l}{\partial t} \Big|_{t=T-t^*, z=R \circ \Phi_l(t^*, z_0)}. \end{aligned}$$

where the last equality follows from the fact that $\Phi_l(0, z_T) = \Phi_l(T - t^*, R \circ \Phi_l(t^*, z_0))$.

Plugging back in, we get the desired result:

$$\begin{aligned}
\left. \frac{\partial t^*}{\partial l_0} \frac{\partial l^{-1}}{\partial z} \right|_{t=T-t^*, z=z_T} \left. \frac{\partial \Phi_l}{\partial t} \right|_{t=T-t^*, z=R \circ \Phi_l(t^*, z_0)} &= - \left. \frac{\partial t^*}{\partial l_0} \frac{\partial l^{-1}}{\partial t} \right|_{t=T-t^*, z=z_T} \\
&= - \frac{1}{v_-^* \top \nabla U_{\text{dif}}(x^*)} \left. \frac{\partial l^{-1}}{\partial t} \right|_{t=T-t^*, z=z_T} \\
&= - \frac{1}{v_-^* \top \nabla U_{\text{dif}}(x^*)} R_{x^*} (v_-^*) \top \nabla U_{\text{dif}}(x^*) \\
&= 1.
\end{aligned}$$

Therefore $w^\top M^{-1}u = -2$, and so

$$|\det(J)| = |(1 + w^\top M^{-1}u) \det(M)| = |(1 - 2)(1)| = 1. \quad \square$$

2 Proof of Theorem 3

Proof. Let x_0 and v_0 denote the initial position and velocity, and let $\{\varepsilon_n\}_{n=0,1,2,\dots}$ and $\{w_t\}_{t>0}$ be a collection of independent exponential random variables with unit rate. Both our bouncy Hamiltonian dynamics and the PDMP will use the same surrogate Hamiltonian dynamics from the same initial position and velocity. We will couple the two processes together through ε_n , which will be used both for the inertia refreshments of the bouncy Hamiltonian dynamics and for the simulation of the inhomogeneous Poisson process for the PDMP. The w_t will be used for additional bounces by the PDMP.

First we construct the bouncy Hamiltonian dynamics with periodic inertia refreshment at Δt intervals. We denote its position, velocity, and inertia components at time t as $\{x^H(t), v^H(t), l^H(t)\}$. Set $x^H(0) = x_0$, $v^H(0) = v_0$, and $l^H(0) = \varepsilon_0$. From time 0 to Δt , the position and velocity evolve according to the surrogate dynamics and the inertia evolves according to Equation (8) in the main text. Then at time Δt , we refresh the inertia by setting $l^H(\Delta t) = \varepsilon_1$, while maintaining the position and velocity. The dynamics then

continues as usual with this new inertia value during $[\Delta t, 2\Delta t]$. We repeat this process for time intervals $[n\Delta t, (n+1)\Delta t]$ for $n = 2, 3, \dots$ until a total travel time of T is achieved.

Now we construct the Hamiltonian PD-MCMC as specified in Vanetti et al. (2017), but with carefully designed coupling to its bouncy Hamiltonian counterpart above. Position and velocity components will be denoted $\{x^P(t), v^P(t)\}$. Again, we set $x^P(0) = x_0$ and $v^P(0) = v_0$. The process travels according to the surrogate Hamiltonian dynamics until the earlier of Δt or the first event at time $\tau_0^{(1)}$, determined by the same exponential variable ε_0 used by the modified bouncy Hamiltonian dynamics:

$$\tau_0^{(1)} = \inf_{t>0} \left\{ \varepsilon_0 = \int_0^t [v^P(s)^\top \nabla U \{x^P(s)\}]^+ ds \right\}.$$

If $\tau_0^{(1)} \leq \Delta t$, then at time $\tau_0^{(1)}$ the velocity is reflected:

$$v^P(\tau_0^{(1)}) = R_{x^P(\tau_0^{(1)})} \{v_-^P(\tau_0^{(1)})\}.$$

The process then continues until time Δt or the next event at time $\tau_0^{(2)} = \tau_0^{(1)} + t_0^{(2)}$, determined now by the w_t :

$$t_0^{(2)} = \inf_{t>0} \left\{ w_{\tau_0^{(1)}} = \int_{\tau_0^{(1)}}^t [v^P(s)^\top \nabla U \{x^P(s)\}]^+ ds \right\}.$$

If $\tau_0^{(2)} \leq \Delta t$, another reflection occurs. Additional bounces are computed and occur until the point where the next bounce time $\tau_0^{(k)}$ is greater than Δt , at which point no further bounces occur on $[0, \Delta t]$. This defines the dynamics on $[0, \Delta t]$, which is repeated for $[n\Delta t, (n+1)\Delta t]$ for $n = 1, 2, \dots$

While the processes are related by ε_0 in determining the first bounce, subsequent bounces by the PDMP are dictated by the w_t and bear no relation to its bouncy Hamiltonian counterpart. In order to keep the processes connected, at each time Δt we define the first event time within the interval $[n\Delta t, (n+1)\Delta t]$ as $\tau_n^{(1)} = n\Delta t + t_n^{(1)}$, where

$$t_n^{(1)} = \inf_{t>0} \left\{ l^H(n\Delta t) = \varepsilon_n = \int_{n\Delta t}^t [v^P(s)^\top \nabla U \{x^P(s)\}]^+ ds \right\}.$$

Thus, the bounce time calculations are regularly connected through the shared use of the ε_i 's.

We now show that the probability these two processes follow the same path converges to 1 as $\Delta t \rightarrow 0$.

$$\begin{aligned}
& \mathbb{P}\{(x_{\Delta t}^H, v_{\Delta t}^H) \equiv (x_{\Delta t}^P, v_{\Delta t}^P) \text{ on } [0, T]\} \\
& \leq \mathbb{P}\{(x_{\Delta t}^H, v_{\Delta t}^H) \equiv (x_{\Delta t}^P, v_{\Delta t}^P) \text{ on } [0, \lceil T/\Delta t \rceil \Delta t]\} \\
& = \prod_{n=0}^{\lceil T/\Delta t \rceil} \mathbb{P}\{(x_{\Delta t}^H, v_{\Delta t}^H) \equiv (x_{\Delta t}^P, v_{\Delta t}^P) \text{ on } [n\Delta t, (n+1)\Delta t] \mid (x_{\Delta t}^H, v_{\Delta t}^H) \equiv (x_{\Delta t}^P, v_{\Delta t}^P) \text{ on } [0, n\Delta t]\} \\
& = \prod_{n=0}^{\lceil T/\Delta t \rceil} \mathbb{P}\{(x_{\Delta t}^H, v_{\Delta t}^H) \equiv (x_{\Delta t}^P, v_{\Delta t}^P) \text{ on } [n\Delta t, (n+1)\Delta t] \mid (x_{\Delta t}^H, v_{\Delta t}^H)(n\Delta t) = (x_{\Delta t}^P, v_{\Delta t}^P)(n\Delta t)\}.
\end{aligned}$$

The last equality follows from the Markov property of the processes. Now we apply Lemma 1 to the last expression:

$$\begin{aligned}
& \prod_{n=0}^{\lceil T/\Delta t \rceil} \mathbb{P}\{(x_{\Delta t}^H, v_{\Delta t}^H) \equiv (x_{\Delta t}^P, v_{\Delta t}^P) \text{ on } [n\Delta t, (n+1)\Delta t] \mid (x_{\Delta t}^H, v_{\Delta t}^H)(n\Delta t) = (x_{\Delta t}^P, v_{\Delta t}^P)(n\Delta t)\} \\
& \geq (1 - C_T(x_0, v_0)\Delta t^2)^{\lceil T/\Delta t \rceil} \\
& \geq (1 - C_T(x_0, v_0)\Delta t^2)^{T/\Delta t + 1} \\
& \geq 1 - C_T(x_0, v_0)(T + \Delta t)\Delta t.
\end{aligned}$$

As we take $\Delta t \rightarrow 0$, this quantity goes to 1 as desired.

□

Lemma 1. *Define finite constants $M \geq \max_{t \leq \Delta t} \{\|x_t\|, \|v_t\|\}$ and D per Lemma 2. Further define*

$$\begin{aligned}
\kappa_{\Delta t}(x, v) &= \max_{x' \in B_{M\Delta t}(x)} [\sigma\{\nabla^2 U_{\text{dif}}(x')\}] \\
L_{\Delta t}(x, v) &= \max_{x' \in B_{M\Delta t}(x)} \{\|\nabla U_{\text{dif}}(x')\|\}
\end{aligned}$$

$$\gamma_{\Delta t}(x_0, v_0) = M^2 \kappa_{\Delta t}(x, v) + DL_{\Delta t}(x_0, v_0)(M + 1)$$

$$C_t(x, v) = \max\{3\gamma_{\Delta t}(x_0, v_0), M^2 L_{\Delta t}(x_0, v_0)^2\},$$

where $B_{M\Delta t}(x)$ is the L^2 ball around x of radius $M\Delta t$ subsuming all locations the chains can possibly reach by time t and $\sigma(A)$ is the largest singular value of A . Then,

$$\begin{aligned} P\{(x_{\Delta t}^H, v_{\Delta t}^H) \equiv (x_{\Delta t}^P, v_{\Delta t}^P) \text{ on } [n\Delta t, (n+1)\Delta t] \mid (x_{\Delta t}^H, v_{\Delta t}^H)(n\Delta t) = (x_{\Delta t}^P, v_{\Delta t}^P)(n\Delta t)\} \\ \geq 1 - C_{\Delta t}(x_n, v_0)\Delta t^2. \end{aligned} \quad (\text{S1})$$

Proof. As the conditioning in the probability in Equation (S1) ensures that the two chains are in identical states at the start of each interval, the proof for each interval $[n\Delta t, (n+1)\Delta t]$ will be the same. We thus assume without loss of generality that $n = 0$ and only consider the interval $[0, \Delta t]$.

Our proof relies on bounding the probability of the chains diverging in cases based on the magnitude of the initial directional derivative $v_0^\top \nabla U(x_0)$. En route to establishing these bounds, we first note the following inequality for the difference of the directional derivatives:

$$\begin{aligned} |v_s^\top \nabla U_{\text{dif}}(x_s) - v_0^\top \nabla U_{\text{dif}}(x_0)| &= |v_s^\top \nabla U_{\text{dif}}(x_s) - v_s^\top \nabla U_{\text{dif}}(x_0) + v_s^\top \nabla U_{\text{dif}}(x_0) - v_0^\top \nabla U_{\text{dif}}(x_0)| \\ &\leq |v_s^\top (\nabla U_{\text{dif}}(x_s) - \nabla U_{\text{dif}}(x_0))| + |(v_s - v_0)^\top \nabla U_{\text{dif}}(x_0)| \\ &\leq \|v_s\| \|\nabla U_{\text{dif}}(x_s) - \nabla U_{\text{dif}}(x_0)\| + \|v_s - v_0\| L_{\Delta t}(x, v_0) \\ &= \|v_s\| \left\| \int_0^s v_u^\top \nabla^2 U_{\text{dif}}(x_u) du \right\| + L_{\Delta t}(x_0, v_0) \left\| \int_0^s -\nabla U_{\text{sur}}(x_u) du \right\| \\ &\leq \|v_s\| \int_0^s \|v_u^\top \nabla^2 U_{\text{dif}}(x_u)\| ds + L_{\Delta t}(x_0, v_0) \int_0^s \|-\nabla U_{\text{sur}}(x_u)\| du \\ &\leq \|v_s\| \int_0^s \|v_u\| \kappa_{\Delta t}(x_0, v_0) du + L_{\Delta t}(x_0, v_0) \int_0^s (D\|x_u\| + D) du \\ &\leq sM^2 \kappa_{\Delta t}(x, v) + L_{\Delta t}(x_0, v_0) sD(M + 1) \\ &\leq \Delta t [M^2 \kappa_{\Delta t}(x, v) + DL_{\Delta t}(x_0, v_0)(M + 1)]. \end{aligned}$$

Define $\gamma_{\Delta t}(x_0, v_0) = M^2 \kappa_{\Delta t}(x, v) + DL_{\Delta t}(x_0, v_0)(M + 1)$, so we have

$$|v_s^\top \nabla U_{\text{dif}}(x_s) - v_0^\top \nabla U_{\text{dif}}(x_0)| \leq \Delta t \gamma_{\Delta t}(x_0, v_0). \quad (\text{S2})$$

If there is one bounce at time t^* , at which point we have new velocity v^* at position x^* , then for $s \in [0, \Delta t - t^*]$ we denote the subsequent trajectory as (v_s^*, x_s^*) . Through an identical calculation, we get the same bound:

$$|v_s^{*\top} \nabla U_{\text{dif}}(x_s^*) - v^{\top} \nabla U_{\text{dif}}(x^*)| = \Delta t \gamma_{\Delta t}(x_0, v_0). \quad (\text{S3})$$

Now we consider two cases,

$$|v_0^\top \nabla U_{\text{dif}}(x_0)| \leq 2\Delta t \gamma_{\Delta t}(x_0, v_0) \quad (\text{S4a})$$

$$|v_0^\top \nabla U_{\text{dif}}(x_0)| > 2\Delta t \gamma_{\Delta t}(x_0, v_0). \quad (\text{S4b})$$

Consider Case (S4a). Then Equation (S2) implies $|v_s^\top \nabla U_{\text{dif}}(x_s)| \leq 3\Delta t \gamma_{\Delta t}(x_0, v_0)$, and so we can bound the probability that the PDMP bounces at least once, which is required for the chains to diverge, as follows.

$$\begin{aligned} \mathbb{P} \left[\varepsilon_0 \leq \int_0^{\Delta t} [v_s^\top \nabla U_{\text{dif}}(x_s)]^+ ds \right] &\leq \mathbb{P} \left[\varepsilon_0 \leq \int_0^{\Delta t} |v_s^\top \nabla U_{\text{dif}}(x_s)| ds \right] \\ &\leq \mathbb{P} \left[\varepsilon_0 \leq \int_0^{\Delta t} 3\Delta t \gamma_{\Delta t}(x_0, v_0) ds \right] \\ &= \mathbb{P}[\varepsilon_0 \leq 3\Delta t^2 \gamma_{\Delta t}(x_0, v_0)] \\ &= 1 - e^{-3\Delta t^2 \gamma_{\Delta t}(x_0, v_0)} \\ &\leq 3\Delta t^2 \gamma_{\Delta t}(x_0, v_0). \end{aligned} \quad (\text{S5})$$

Now Consider Case (S4b). If $v_0^\top \nabla U_{\text{dif}}(x_0) < -2\Delta t \gamma_{\Delta t}(x_0, v_0)$, Equation (S2) implies $v_s^\top \nabla U_{\text{dif}}(x_s) < -\Delta t \gamma_{\Delta t}(x_0, v_0) < 0$, and so neither chain bounces.

If $v_0^\top \nabla U_{\text{dif}}(x_0) > 2\Delta t \gamma_{\Delta t}(x_0, v_0)$, Equation (S2) implies $v_s^\top \nabla U_{\text{dif}}(x_s) > \Delta t \gamma_{\Delta t}(x_0, v_0) > 0$, so they either both don't bounce, in which case they don't diverge, or they share the first

bounce. If they share first bounce, they diverge only if they bounce again. Consider the probability the bouncy Hamiltonian dynamics bounce again. Equation (S3) implies that $v^{*\top} \nabla U_{\text{dif}}(x^*)$ and $v_s^{*\top} \nabla U_{\text{dif}}(x_s^*)$ share the same sign if $|v^{*\top} \nabla U_{\text{dif}}(x^*)| > \Delta t \gamma_{\Delta t}(x_0, v_0)$, which is implied since $|v^{*\top} \nabla U_{\text{dif}}(x^*)| = |v_{t^*}^\top \nabla U_{\text{dif}}(x_{t^*})| > \Delta t \gamma_{\Delta t}(x_0, v_0)$. Then since $v^{*\top} \nabla U_{\text{dif}}(x^*) = -v_{t^*}^\top \nabla U_{\text{dif}}(x_{t^*}) < 0$, no additional bounces occur. Now consider probability the PDMP bounces at least twice, which we decompose into the conditional probability that it bounces at least twice given at least one bounce, times the probability of at least one bounce:

$$\begin{aligned}
& \mathbb{P} \left[w_{t^*} \leq \int_0^{\Delta t - t^*} [v_s^{*\top} \nabla U_{\text{dif}}(x_s^*)]^+ ds \right] \mathbb{P} \left[\varepsilon_0 \leq \int_0^{t^*} [v_s^\top \nabla U_{\text{dif}}(x_s)]^+ ds \right] \\
& \leq \mathbb{P} \left[w_{t^*} \leq \int_0^{\Delta t - t^*} |v_s^{*\top} \nabla U_{\text{dif}}(x_s^*)| ds \right] \mathbb{P} \left[\varepsilon_0 \leq \int_0^{t^*} |v_s^\top \nabla U_{\text{dif}}(x_s)| ds \right] \\
& \leq \mathbb{P} \left[w_{t^*} \leq \int_0^{\Delta t - t^*} \|v_s^*\| \|\nabla U_{\text{dif}}(x_s^*)\| ds \right] \mathbb{P} \left[\varepsilon_0 \leq \int_0^{t^*} \|v_s\| \|\nabla U_{\text{dif}}(x_s)\| ds \right] \\
& \leq \mathbb{P} \left[w_{t^*} \leq \int_0^{\Delta t - t^*} ML_{\Delta t}(x_0, v_0) ds \right] \mathbb{P} \left[\varepsilon_0 \leq \int_0^{t^*} ML_{\Delta t}(x_0, v_0) ds \right] \tag{S6} \\
& \leq \mathbb{P}[w_{t^*} \leq (\Delta t - t^*) ML_{\Delta t}(x_0, v_0)] \mathbb{P}[\varepsilon_0 \leq t^* ML_{\Delta t}(x_0, v_0)] \\
& \leq \mathbb{P}[w_{t^*} \leq \Delta t ML_{\Delta t}(x_0, v_0)] \mathbb{P}[\varepsilon_0 \leq \Delta t ML_{\Delta t}(x_0, v_0)] \\
& \leq (1 - e^{-\Delta t ML_{\Delta t}(x_0, v_0)}) (1 - e^{-\Delta t ML_{\Delta t}(x_0, v_0)}) \\
& \leq \Delta t^2 M^2 L_{\Delta t}(x_0, v_0)^2.
\end{aligned}$$

Combining our results, we have that the probability of diverging is bounded by the larger of the last expression of Equation (S5) and (S6). \square

Lemma 2. Assume $U_{\text{sur}}(x)$ is twice continuously differentiable and $\limsup_{\|x\| \rightarrow \infty} \frac{\|\nabla U_{\text{sur}}(x)\|}{\|x\|} < \infty$. Then, the solution of bouncy Hamiltonian dynamics satisfies

$$\max\{\|x_t\|^2, \|v_t\|^2\} \leq e^{(D+1)t}[(\|x\| + 1)^2 + \|v\|^2]$$

for any $t \geq 0$ with constant $D < \infty$.

Proof. The fact that $\|\nabla U_{\text{sur}}(x)\| < D\|x\| + D$ directly follows from the assumptions. Consider the function $(\|x_t\| + 1)^2 + \|v_t\|^2$. We will bound it using Gronwall's inequality, which in

turn will let us bound $\|x_t\|$ and $\|v_t\|$. First, assume there are no bounces and let $s \in [0, \Delta t]$.

Then we have the following bound:

$$\begin{aligned}
\frac{d}{dt} [(\|x_s\| + 1)^2 + \|v_s\|^2] &= \left[2(\|x_s\| + 1) \frac{x_s}{\|x_s\|} \right]^\top v_s + 2v_s^\top \nabla U_{\text{sur}}(x_s) \\
&= 2 \left[x_s^\top v_s + \frac{x_s^\top v_s}{\|x_s\|} + v_s^\top \nabla U_{\text{sur}}(x_s) \right] \\
&\leq 2 \left[\|x_s\| \|v_s\| + \frac{\|x_s\| \|v_s\|}{\|x_s\|} + \|v_s\| \|\nabla U_{\text{sur}}(x_s)\| \right] \\
&= 2(\|x_s\| \|v_s\| + \|v_s\| + \|v_s\| \|\nabla U_{\text{sur}}(x_s)\|) \\
&\leq 2[\|x_s\| \|v_s\| + \|v_s\| + \|v_s\|(D\|x_s\| + D)] \\
&= 2(D + 1)(\|x_s\| \|v_s\| + \|v_s\|) \\
&\leq (D + 1)[(\|x_s\| + 1)^2 + \|v_s\|^2].
\end{aligned}$$

By Gronwall's inequality, we have

$$\begin{aligned}
(\|x_s\| + 1)^2 + \|v_s\|^2 &\leq e^{(D+1)s} [(\|x_0\| + 1)^2 + \|v_0\|^2] \\
&\leq e^{(D+1)\Delta t} [(\|x_0\| + 1)^2 + \|v_0\|^2].
\end{aligned} \tag{S7}$$

Now assume we have one bounce at time t^* , at which point we have new velocity v^* at position x^* . Then for $s \in [0, \Delta t - t^*]$, we again denote the trajectory as (v_s^*, x_s^*) . We can repeat a similar procedure as before to obtain the following bound:

$$\frac{d}{dt} [(\|x_s^*\| + 1)^2 + \|v_s^*\|^2] \leq (D + 1)[(\|x_s^*\| + 1)^2 + \|v_s^*\|^2].$$

Combining Gronwall's inequality and Equation (S7), we get the same bound as Equation (S7):

$$\begin{aligned}
(\|x_s^*\| + 1)^2 + \|v_s^*\|^2 &\leq e^{(D+1)s} [(\|x^*\| + 1)^2 + \|v^*\|^2] \\
&\leq e^{(D+1)(\Delta t - t^*)} e^{(D+1)t^*} [(\|x_0\| + 1)^2 + \|v_0\|^2] \\
&= e^{(D+1)\Delta t} [(\|x_0\| + 1)^2 + \|v_0\|^2].
\end{aligned} \tag{S8}$$

The recursive procedure in the second line of Equation (S8) can be extended to arbitrary number of bounces in straightforward fashion, and so the desired result follows directly. \square

3 Proof of Theorem 4

Proof. To argue by contradiction, assume such a momentum distribution $\pi(p)$ exists and choose a starting state (x_0, p_0) . In order to accommodate the discontinuous nature of the velocities resulting from bounces, we require a more general definition of Hamiltonian dynamics that includes the assumption that the dynamics stay away from a measure 0 set. This assumption parallels the assumption required in Theorem (1) to ensure that Equation (1) has a unique solution by avoiding cases, where, for example, the bounces are not well defined. We avoid the sets:

$$\{(x, p) : \nabla U = 0\}, \quad \{(x, p) : \nabla K^\top \nabla U = v^\top \nabla U = 0\}.$$

and further assume p_0 does not lie on a boundary between pieces so the first bounce is not instantaneous.

We will first show that we can find a neighborhood around the initial state such that according to Hamiltonian dynamics, the velocities after the first bounce are identical. Denote the position and momentum at the first bounce time as (x^*, p^*) and the velocity immediately after the bounce as v^* . Crucially, from Lemma 3 we know that $\pi(p)$ is piecewise exponential and so velocity is constant on each of these pieces, with changes in velocity occurring when boundaries between pieces are crossed. By continuity of these boundaries as well as local continuity of Hamiltonian dynamics around (x_0, p_0) , it is straightforward to find a δ such that for all $(\tilde{x}_0, \tilde{p}_0) \in B_\delta(x_0, p_0)$, $\tilde{v}^* = v^*$.

Now we show that the property of the Hamiltonian dynamics we have just established is impossible under HBPS dynamics. Specifically, we show that if the trajectory were to bounce off the hyperplane orthogonal to ∇U , the post-bounce velocity \tilde{v}^* necessarily differs from v^* for almost every initial condition in a neighborhood of (x_0, v_0) .

Consider the function f which takes $(\tilde{x}_0, \tilde{p}_0)$ and returns the difference between \tilde{v}^* and

v^* :

$$f(\tilde{x}_0, \tilde{p}_0) = v_0 - 2 \frac{v_0^\top \tilde{x}^*}{\|\tilde{x}^*\|^2} \tilde{x}^* - v^*,$$

where \tilde{x}^* is the position at bounce time. The set of initial states in $B_\delta(x_0, p_0)$ where $\tilde{v}^* = v^*$ can be written

$$\{(\tilde{x}_0, \tilde{p}_0) \in B_\delta(x_0, p_0) : f(\tilde{x}_0, \tilde{p}_0) = 0\}.$$

By the implicit function theorem, this set is a manifold of dimension less than $2d$, and thus has measure 0, as long as the Jacobian of f evaluated at (x_0, p_0) is not 0. This Jacobian can be written

$$\left[\begin{array}{cc} \frac{\partial f}{\partial \tilde{x}_0} & \frac{\partial f}{\partial \tilde{p}_0} \end{array} \right] \Big|_{\tilde{x}_0=x_0, \tilde{p}_0=p_0}$$

and it suffices to evaluate the first term, which is the product of three matrices:

$$\begin{aligned} & \frac{\partial f}{\partial \tilde{x}_0} \Big|_{\tilde{x}_0=x_0, \tilde{p}_0=p_0} \\ &= \left[\frac{-2}{\|\nabla U(\tilde{x}^*)\|^2} \left(\nabla U(\tilde{x}^*) v_0^\top - 2v_0^\top \nabla U(\tilde{x}^*) \frac{\nabla U(\tilde{x}^*) \nabla U(\tilde{x}^*)^\top}{\|\nabla U(\tilde{x}^*)\|^2} + v_0^\top \nabla U(\tilde{x}^*) I \right) \right. \\ & \quad \left. \times \nabla^2 U(\tilde{x}^*) \left(I + v_0 \frac{\partial t^*}{\partial \tilde{x}_0} \right) \right] \Big|_{\tilde{x}_0=x_0, \tilde{p}_0=p_0} \end{aligned}$$

The Hessian $\nabla^2 U$ is full rank since U is strongly convex, and the other matrices are rank $d-1$ since they are rank-one perturbations of the identity matrix. Therefore their product is at least rank $d-2$, so it cannot be 0 when $d \geq 3$.

□

Lemma 3. *If a Hamiltonian dynamics were to follow a piecewise linear trajectory under a strongly log-concave $\pi(x)$ and piecewise smooth $\pi(p)$, then $\pi(p)$ must be piecewise exponential.*

Proof. Since velocity changes in a discontinuous fashion when crossing the boundaries of the pieces of $\pi(p)$ and must be constant otherwise, this suggests that the pieces of $\pi(p)$ are

piecewise exponential. However, from a given starting state, we only guarantee that ∇K is constant along the one dimensional trajectory traced by the dynamics. To extend this to the entire piece, we will perturb the position component to adjust the trajectory while keeping the momentum, and thus velocity, constant. We show that for any momentum chosen in the interior of a piece, we can find a neighborhood around it such that each element can be reached by a perturbation in the position alone, implying ∇K must be constant on this neighborhood. This, in conjunction with the piecewise continuous nature of ∇K arising from the piecewise smoothness of $\pi(p)$ will imply that $\pi(p)$ is piecewise exponential.

More formally, take any state (x, p) away from the discontinuities in $\pi(p)$. Equation (1) and the requirement that velocities be piecewise constant imply that $v = \nabla K(p)$ is constant for $p_t = p + \int_0^t \nabla U(x + sv) ds$ and $p_t = p + \int_0^t \nabla U(x - sv) ds$ for sufficiently small t . Consider the initial state $(x_0, p_0) = (x - tv, p - \int_0^t \nabla U(x - tv + sv) ds)$, which arrives at (x, p) when advanced for time t .

Now consider the function $p_t(\tilde{x}_0)$ which fixes p_0 , takes a position \tilde{x}_0 as an argument, and returns the momentum after evolving the dynamics for time t . If we can show that the Jacobian of this function evaluated at x_0 is full rank, the inverse function theorem implies that there exists a neighborhood around x_0 which maps bijectively to a neighborhood around $p_t(x_0) = p$ as desired.

By definition of the dynamics, we have

$$p_t(\tilde{x}_0) = p_0 + \int_0^t \nabla U(\tilde{x}_0 + sv) ds$$

with Jacobian evaluated at x_0 given by

$$\int_0^t \nabla^2 U(x_0 + sv) ds.$$

Since U is strongly convex, $\nabla^2 U$ is positive definite and thus the Jacobian is full rank. \square

References

- Nishimura, A., Zhang, Z., and Suchard, M. A. (2024). Zigzag path connects two Monte Carlo samplers: Hamiltonian counterpart to a piecewise deterministic Markov process. *arXiv preprint arXiv:2104.07694*.
- Spivak, M. (1965). *Calculus on manifolds: a modern approach to classical theorems of advanced calculus*. CRC press.
- Vanetti, P., Bouchard-Côté, A., Deligiannidis, G., and Doucet, A. (2017). Piecewise-deterministic Markov chain Monte Carlo. *arXiv preprint arXiv:1707.05296*.